国際化推進共同研究概要

No.12

タイトル: Development of microphysical model of cirrus clouds used for lidar and radar sounding

研究代表者: BOROVOY, ANATOLY, GEORGIEVICH

所内世話人: 岡本 創

実施期間: 2017年3月23日 ～ 3月31日

研究概要: 衛星搭載ライダによって観測される氷雲からの後方散乱の情報を解釈するために、従来より格段に計算精度の高い手法である、物理光学手法を開発した。2016年度は、1mm程度の大粒子に対しても、計算可能な改良を実施した。ライダの鉛直下向きからの傾斜角が0.3度の場合と3度の場合の衛星解析用の参照テーブルを作成するため、氷粒子の形状と配向を考慮した10ミクロンから1mmまでのサイズに対する波長532nmと1064nmに対する後方散乱光の計算を行う予定である。

No. 12 Development of a microphysical model of cirrus clouds used lidar and radar sounding.

Institute of Atmospheric Optics, Rus.Acad. Sci., Prof. A.G. Borovoy

Aim:

At both lidar and radar soundings of cirrus clouds, the backscattering Mueller matrix has been measured. This is the backscattering Mueller matrix that are used for retrieving such microphysical properties of cirrus clouds as sizes, shapes and spatial orientation of the ice crystals constituting the clouds. This retrieval is based on the theoretical solution of lidar and radar scattering by one ice crystal averaged over the statistical ensemble. For radars, this solution had been successfully obtained by the RIAM team (Okamoto et al., 2010, Sato and Okamoto 2011) where radar signals were calculated by the reliable numerical methods (DDA, FTDT). Here the crystal sizes are ranging from several microns up to 10 000 microns. However, there were no reliable methods to calculate light backscatter by ice crystals of cirrus clouds. Only in the last years, the IAO team has developed such a method called the physical-optics approximation. At present the method was applicable only to the small fraction of the crystals with sizes less than 1000 microns. The aim of the project is to create the data bank for the backscattering matrixes of the ice crystals with different shapes restricting for lidars by sizes up to 1000 microns.

The heads of the teams Prof. H. Okamoto and Prof. A. Borovoi began their joint development of this scientific direction when Prof. A. Borovoi was a visiting researcher in RIAM for 3 months in 2011.

Method:

The problem of light scattering by such large particles as ice crystals of cirrus clouds is a vibrant problem of the atmospheric optics that is just under developing. Here the standard methods for solutions to the exact Maxwell equations prove to be computationally expensive for the ice crystals of cirrus clouds. Some new methods such as Pseudo-spectral time-domain method (PSTD) (Ping Yang at al., 2013) and Invariant embedding T-matrix method (Bi et al., 2014) were suggested but these methods prove to be capable to solve the problem for the ice crystal of sizes up to 20 micrometers for the visible yet while the ice crystal sizes range from a few micron up to millimeter. In particular, in two recent papers 1) Chen Zhou and Ping Yang, "Backscattering peak of ice cloud particles," Opt. Exp. v.23, 11995, 2015 and 2) Jiachen Ding, Ping Yang, Robert E. Holz, Steven Platnick, Kerry G. Meyer, Mark A. Vaughan,Yongxiang Hu, and Michael D. King, "Ice cloud backscatter study and comparison with CALIPSO and MODIS satellite data," Opt. Exp. v. 24, 620, 2016, these leading scientists confirmed that their algorithms are not capable to calculate the light backscattering from cirrus clouds and they needed to use some artificial procedures to guess the backscatter used for interpretation of lidar signals.

The main obstacle for the abovementioned calculations was the large magnitude of the ratio of (particle size/wavelength) that resulted in computationally expensive calculations. However, there is a method that is practically independent of this ratio. This is the physical-optics method. It was begun by Borovoi et al. in 2003 and then it had been improving for last years. In particular, the algorithms of the geometric-optics and physical-optics methods have been opened for free access and the approximations have been discussed in details in two recent papers of 2016: 1) Konoshonkin A.V., Kustova N.V., Borovoi A.G., Grynko Y., Förstner J. , "Light scattering by ice crystals of cirrus clouds: Comparison of the physical optics methods" Journal of Quantitative Spectroscopy and Radiative Transfer V.182, P. 12-23.
2) Konoshonkin A.V. , Borovoi A.G., Kustova N.V., Okamoto H., Ishimoto H., Grynko Y., Förstner J. "Light scattering by ice crystals of cirrus clouds: from exact numerical methods to physical-optics approximation" Journal of Quantitative Spectroscopy and Radiative Transfer

(Accepted 2017, DOI: 10.1016/j.jqsrt.2016.12.024) . In these papers, the method of the physical optics has been compared with two the numerically exact methods and it was proven that it is quite reliable.

Simulations in 2016:

In 2016, the IAO team has completed the data base for the light backscattering Mueller matrixes for the following quantities:
Wavelengths: 0.532 μm and 1.064 μm

- Refractive indices: 1.3116 and 1.3004, respectively.
- Lidar zenith angles: 0.3° and 3°
- Particle shapes: hexagonal columns and plates with size-dependent aspect ratios according Mitchell and Arnott [J. Atmos. Sci. 1994. V. 51. P. 817–832].
- Particle dimensions
  columns: 27 discrete of length, from 10 to 1000 micron
  plates: 21 discrete of diameter, from 10 to 1000 micron
- Particle orientations: 362 discrete, from fully horizontally aligned to completely random.
- Particles shape:
  plates: regular hexagonal prism
  columns: regular hexagonal prism and irregular hexagonal prism with the distortion angle of 0.25°.

Joint publications:

1. Konoshonkin A.V., Borovoi A.G., Kustova N.V., Okamoto H., Ishimoto H., Grynko Y., Förstner J. "Light scattering by ice crystals of cirrus clouds: from exact numerical methods to physical-optics approximation" Journal of Quantitative Spectroscopy and Radiative Transfer (Accepted 2017, DOI: 10.1016/j.jqsrt.2016.12.024)

2. Konoshonkin A.V., Kustova N.V., Borovoi A.G., Okamoto H. , Sato K. , Ishimoto H., Grynko E. , Förstner J., " Comparison between the physical-optics approximation and exact methods solving the problem of light scattering by ice crystals of cirrus clouds", Proceedings of SPIE. 2016. V.10035. CID: 1003 33. [10035–26].

3. Konoshonkin A.V., Borovoi A.G., Kustova N.V., Okamoto H., Sato K. "Optical and microphysical properties of cirrus clouds retrieved from combined lidar and radar measurements" Proceedings of SPIE. 2016. V.10035. CID: 1003 3X. [10035–126].

国際化推進共同研究概要

No.13

タイトル: Water mass modification in the Japan Sea and East Asian marginal seas

研究代表者: SHIN, Hong-Ryeol

所内世話人: 千手 智晴

実施期間: 2017年2月13日～月日日

研究概要: 日本海大和海盆の南縁に流速計を係留し、深層流の直接測流を実施した。
係留作業は2016年10月5～15日に、長崎大学の長崎丸を用いて行い、同時にCTDによる密度場の観測も行った。流速計の回収は2017年5月の予定である。
2017年2月13日に九州大学応用力学研究所において"International Workshop on Mixing and Water Mass Modification in the East Asian Marginal Seas"を開催した。
日本・韓国・中国の研究者による、主に東シナ海、日本海の海水循環・海水混合に関する8題の研究発表があり、参加者は21名であった。

Research Report

Water mass modification in the Japan Sea and East Asian marginal seas

Hong-Ryeol Shin (Kongju National University)
Tomoharu Senjyu (RIAM, Kyushu University)

Aim of this research

Long-term trends of warming and decreasing concentration in dissolved oxygen have been reported in the abyssal Japan/East Sea, and the relationship to global warming has been pointed out. In particular, dissolved oxygen concentration is decreasing at a rate of 1.0 μmol kg^{-1} $year^{-1}$, which is very high rate in the world, and the influence for the material cycle and biological activity in the whole Japan/East Sea are concerned. The structural changes in the deep water of the Japan/East are considered to affect on the material distribution and biological activity through the changes in circulation. We investigate the relationship between deep water circulation and distribution of water characteristics by field observations.

Water mass modification associated with global warming and climate change has been reported from the other East Asian marginal seas, such as the East China Sea, Yellow Sea and the Okhotsk Sea. This fact indicates that the East Asian marginal seas including atmosphere over the seas should be considered as one system. Therefore, we held an international workshop about water mass modification and oceanic mixing processes discussed in the each marginal sea to establish a concept of the East Asian Marginal Seas System.

Results

Direct current observations in the deep Japan/East Sea were carried out using current meters of RIAM Kyushu University. The mooring points are in the southern edge of the Yamato Basin (37°20-25'N, 135°40'E), and the mooring operations were conducted by T/V Nagasaki Maru of Nagasaki University during the period of October 5-15, 2016. Hydrographic observations with CTD were also carried out in the same cruise. These current meters will be recovered in May 2017.

"International Workshop on Mixing and Water Mass Modification in the East Asian Marginal Seas" was held in February 13, 2017 at RIAM, Kyushu University. The conveners were H.-R. Shin and T. Senjyu, and the total participants were 21 persons. As shown in the program below, eight titles about circulation and oceanic mixing processes mainly in the East China Sea and the Japan/East Sea were presented in the workshop by the researchers from Japan, Korea and China. Because this workshop is part of the ceremonial events of Prof. Matsuno's retirement, and a joint workshop about physical, chemical and biological environments in the East China Sea (conveners: Prof. Matsuno and Prof. Ishizaka in Nagoya University) was held in the next day in RIAM, many scientists associated with Prof. Matsuno were participated and active discussions were made.

International Workshop on

Mixing and Water Mass Modification in the East Asian Marginal Seas

February 13, 2017

W601 in Research Institute for Applied Mechanics, Kyushu University

Kasuga, Fukuoka, Japan

Water mass modification as a result of oceanic mixing is one of important factors controlling biogeochemical conditions in the ocean. Marginal seas in the East Asia such as the Yellow, East China and Japan/East Seas are rapidly changing due to natural and anthropogenic multi-timescale variations. The aim of this workshop is to promote studies on the mixing and water mass modification processes in the East Asian area through exchange scientific information. We welcome not only observational and modeling studies about physical processes of the water mass modification, but also about mixing effects on the biogeochemical conditions in the oceans.

10:00-10:05

Opening address

Hong-Ryeol Shin (Kongju National Univ.)

Chair: Hong-Ryeol Shin

10:05-10:35

Enhanced turbulence observed in the East China Sea shelf

Jae Hak Lee (KIOST), Chang Su Hong (KIOST) and Gyu Nam Baek (KIOST)

10:35-11:05

Budget of nutrients and biogenic particles for upper and lower layers of the East China Sea

Yucheng Wang (Ehime Univ.), Xinyu Guo (Ehime Univ.) and Liang Zhao (Tianjin Univ. Sci. Tech.)

----- Coffee Break 11:05-11:20 -----

11:20-11:50

Water exchange across isobaths over the continental shelf of the East China Sea

Jing Zhang (Ehime Univ.), Xinyu Guo (Ehime Univ.), Liang Zhao (Tianjin Univ. Sci. Tech.) and Yasumasa Miyazawa (JAMSTEC)

11:50-12:20

Studies on turbulent mixing and tidal currents in Ariake Sea

Eisuke Tsutsumi (Kyushu Univ.) and Takeshi Matsuno (Kyushu Univ.)

----- Lunch 12:20-14:00 -----

Chair: Jae Hak Lee

14:00-14:30

Trends the appearance of coastal upwelling along the eastern coast of Korea during last a few years

In-Seong Han (NIFS) and Sang-Hyun Kim (Cheju National Univ.)

14:30-15:00

Seasonal characteristics of the circulation in the East/Japan Sea depending on sea surface heat flux

Daehyuk Kim (Kongju National Univ.), Hong-Ryeol Shin (Kongju National Univ.), Cheol-Ho Kim (KIOST) and Naoki Hirose (Kyushu Univ.).

----- Coffee Break 15:00-15:15 -----

15:15-15:45

Evaluation of vertical eddy diffusivity in the abyssal Japan/East Sea based on the one-dimensional advection-diffusion model in temperature and ^{14}C profiles

Tomoharu Senjyu (Kyushu Univ.) and Takafumi Aramaki (NIES)

15:45-16:15

Development of northeast Asian seas regional climatology by quality control of temperature and salinity data from the World Ocean Database

Joon-Soo Lee (NIFS)

Chair: Tomoharu Senjyu

16:15-17:00

Discussion

国際化推進共同研究概要

No.14

タ イ ト ル: Strength and fracture toughness of bonded CFRP laminates fabricated by vacuum-assisted RTM

研究代表者: CHOI, Nak-Sam

所内世話人: 新川 和夫

実 施 期 間: 2017 年 2 月 8 日 ～ 2 月 11 日

研究概要: 真空樹脂含浸法を用いて炭素繊維強化複合材料および接合部を作製し、接合部の強度を曲げ試験により評価した。またアコーステックエミッション法により破壊の進展挙動を計測した。接合方法を縫製および多層接合にすることにより、接合強度がそれぞれ 27%および 112%増加することを明らかにした。

Bending strength of novel CFRP composite adhesive joints fabricated from two dry carbon halves using vacuum assisted resin transfer molding

Mahmoud R. Abusrea[a,b], Seung-Wook Han[c], Kazuo Arakawa[d], Nak-Sam Choi[c*]

[a] Interdisciplinary Graduate School of Engineering Sciences, Kyushu University, Fukuoka 816-8580, Japan

[b] Faculty of Engineering, Cairo University, Giza 12613, Egypt

[c] Department of Mechanical Engineering, Hanyang University, Ansan 426-791, South Korea

[d] Research Institute for Applied Mechanics, Kyushu University, Fukuoka 816-8580, Japan

* Correspondence to: Nak-Sam Choi; e-mail: nschoi@hanyang.ac.kr

Abstract

Composite adhesive joints are commonly used for large, light structures, such as wind turbines, and in ships and aerospace applications. The laminated joint in this work was an adhesive joint composed of two dry carbon fiber halves, manufactured using a vacuum-assisted resin transfer molding (VARTM) process. For this joint, some improvements are provided to enhance performance, in terms of bending strength. These improvements include the stitching of the two halves together using carbon fiber bundles and inserting extra carbon fiber covers in the joint connection. We studied three adhesive joints: a conventional laminated joint and two improved laminated joints. All joints and CFRP fabrics were made in our laboratory using VARTM techniques. Specimens were prepared for bending tests to evaluate joint performance. Two acoustic emission (AE) sensors were placed on the specimen to monitor fracture progress during the test. The results showed a considerable improvement in bending strength for the modified laminated joints. The percentage increases in the bending strength were 27% and 112% for stitched and multiple-cover laminated joints, respectively, for the six-layer laminates.

Keywords— CFRP joints, vacuum-assisted resin transfer molding, bending strength of joints

Introduction

The use of CFRP composite materials in engineering structures brings many advantages because of their high performance and mechanical properties, such as high strength-to-weight and stiffness-to-weight ratios [1]. For this reason, they have been used for heavy duty structures in aviation, space [2-5], automotive [4], shipbuilding [5], and wind turbine applications [6]. These applications generally involve large-scale manufacturing, so the parts are produced from smaller components and are joined together. The mechanical performance of these structures is highly dependent on the joining efficiency.

Because composite joints work as structure-critical load-carrying elements, the design and analysis of

composite joints have attracted much attention in a series of light, low-cost, and efficient composite integration projects [7]. 'Traditional' mechanical fasteners, such as bolts, pins, and rivets, have been used to join CFRP structures [8-10]. This composite joining technique is generally characterized by simplicity and the fact that such joints can be disassembled [11]. However, drilling holes in composite parts before fastening may cause problems due to stress concentration and weight increases. In contrast, adhesively bonded joints have mechanical advantages over bolted joints because the fibers are not cut, and stresses are transmitted more homogeneously [12]. They offer better structural integrity, lower weight, and higher strength-to-weight ratios [13, 14].

Today, adhesive composite joints are used widely in many composite structures in aerospace, turbine, and ship designs [15]. These joints include single-lap [12, 16], double-lap [17, 18], and stepped [19, 20] joints. It is known that these engineering structures are subjected to combinations of mechanical loadings, including static, fatigue, and impact loadings. Many studies have characterized and improved the mechanical performance of these adhesive joints. For example, Lobel et al. [21] showed enhanced tensile strength using z-pinning for CFRP double-lap joints. Another approach for adhesive joint improvement was reported by Nogeira et al. [22]. They used spiked metal sheets placed within the bondline to gain mechanical load transfer. Furthermore, stitching is a technique for reinforcing the laminate. Dransfield et al. [23] and Heb et al. [24] showed that this technique enhanced the fracture toughness of composites. Kim et al. [25] evaluated the fatigue performance of composite stepped lap joints considering the number of steps, joint length, and edge angle of the adherends. They concluded that the fatigue performance was improved by increasing the number of steps and the edge angle.

Using a composite-manufacturing technique referred to as vacuum-assisted resin transfer molding (VARTM; see Fig. 1), we fabricated wind-lens parts for offshore wind power applications [13, 26-28]. This manufacturing technique can be used to fabricate various adhesive joint designs, based on the stacking sequence of the carbon fiber layers. The adhesive joints can be characterized by bending strength when compared with 'conventional' adhesive joints as well as mechanical fasteners [6, 13, 14]. In this study, a novel CFRP adhesive joint, called a "laminated joint," is introduced. This joint was constructed of two mated dry carbon fiber halves. Two modifications were made to the joint. The first was the application of a stitching technique (i.e., a stitched laminated joint) and second was the addition of carbon fiber pieces (i.e., a multiple-covers laminated joint). Figures 2a-d show the joints in the current research. These joints were

subjected to three-point bending tests with acoustic emission (AE) sensors. The major objective of this work was to characterize and improve the bending strength for the modified joints described.

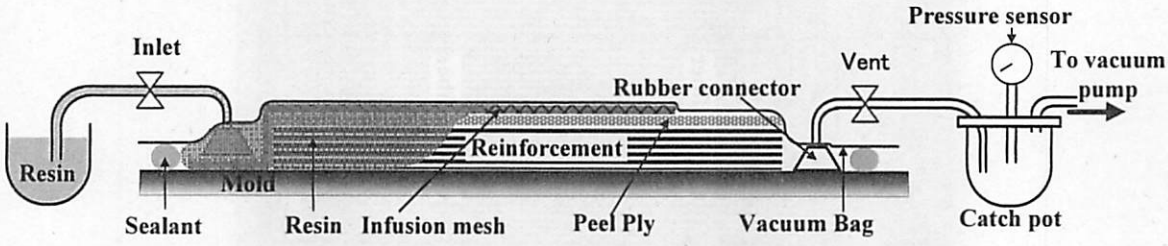

Figure 1: Schematic diagram of the vacuum-assisted resin transfer molding (VARTM) process

Materials and Fabrications

Materials

The CFRP composites consisted of carbon fabric (Mitsubishi Rayon UD 1M; 317 g/m2) and a resin (Denatite XNR6815/XNH6815) [6]. The resin was a mixture of XNR6815 and XNH6815 at a weight ratio of 100:27. The resin mixture viscosity at 25°C was 260 mP.s. The carbon fiber type was TRH50 12L, composed of 12k filaments, with each filament being 7 μm in diameter. The tensile strength, tensile modulus, and elongation percent were 4900 MPa, 253 GPa, and 1.9%, respectively.

Adhesive joints

The laminated joint proposed in this work is a composite adhesive joint constructed of two dry carbon halves that are stacked in mating together. The fiber volume fraction measured for this joint was about 62%. In this joint, the joint length was 40 mm and the total specimen length was 80 mm (Fig. 2b). The first improvement to this joint was made by applying a stitching technique. We used stitching with carbon bundles of the same carbon fiber type, which were applied perpendicular to the plane of the laminate [23, 24]. Figure 2c shows the stitched laminate joint (SLJ). Abusrea and Arakawa [29] showed a weakened stepped joint in which stitching was applied; the tensile strength of the stitched stepped joint was 26% lower. However, it showed improved tensile strength when the stitching was applied to the dry carbon-to-dry carbon joints. The second improvement was made by adding carbon fiber pieces of 40 mm in length. These carbon fiber pieces were put between the carbon fiber layers and covered the contact between the two joint halves. Figure 2d shows the multi-covered laminate joint (MCLJ).

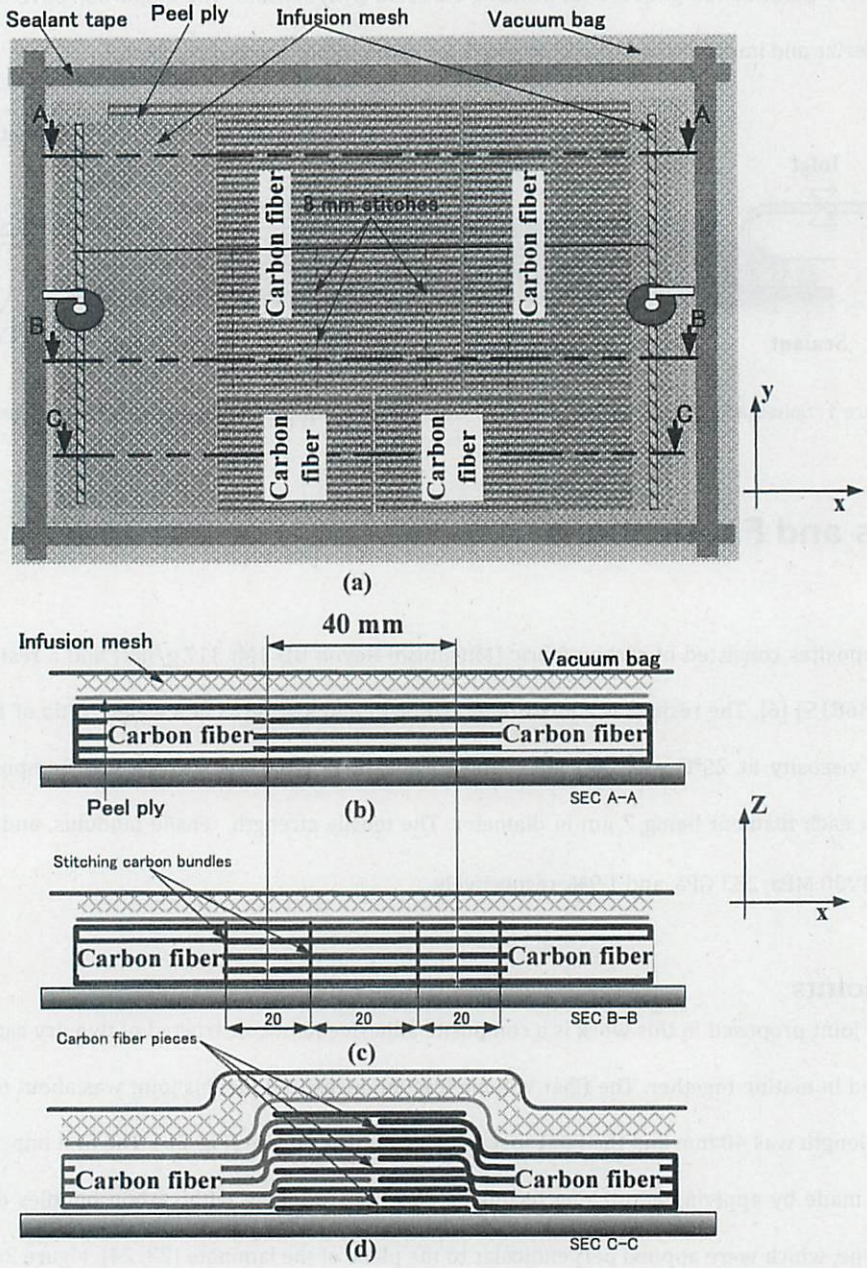

Figure 2: (a) Schematic view of the joints. (b) Sectional side view of the laminated joint (LJ). (c) Sectional side view of the stitched laminated joint (SLJ). (d) Sectional side view of the multiple-cover laminated joint (MCLJ).

In this work, we have chosen 4 different number of carbon fiber layers for all joints. We have assigned 5, 6, 7 and 10 carbon fiber layers because they are commonly used. For the first joint, conventional laminated joint, we had two different cases, so we divided the four number of carbon fiber layers into two combinations which are 6&10 and 5&7 carbon fiber layers. Two cases were examined for the laminated joint: a '*normal case*' laminated joint (NCLJ) and a 'shifted case' laminated joint (SCLJ). For NCLJ, the carbon fiber layers were

stacked and arranged 'correctly' in their positions; that is, there was no gap at the joint ends (Fig. 3a). We used 6 and 10 carbon fiber layers as examples. In the SCLJ, the carbon fiber layers were shifted to create a gap at the joint ends (Figure 3b). Because carbon fiber layer movement may occur during mold preparation with this kind of joint, the SCLJ was used to examine the effects of any such movement on final product quality, in terms of thickness variation, and mechanical performance, in terms of bending strength. For the SCLJ, 5 and 7 carbon fiber layers were stacked.

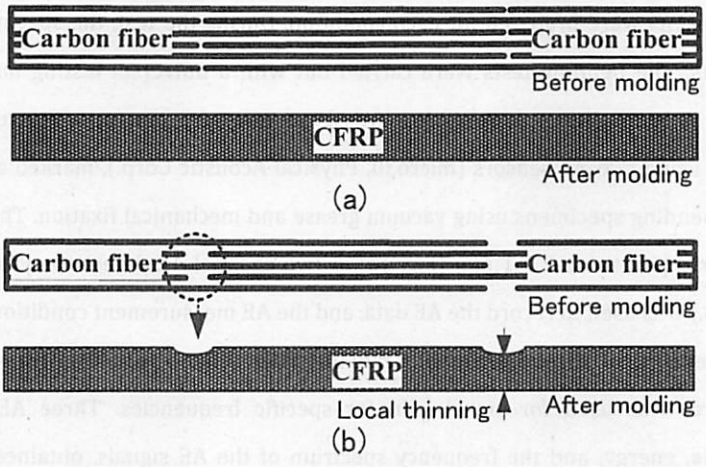

Figure 3: Schematic drawing before and after molding for the (a) normal-case laminated joint (NCLJ) and (b) shifted-case laminated joint (SCLJ).

Manufacturing of CFRP joints

All CFRP fabrics and joints were fabricated using the VARTM set-up shown in Figure 1. Composite fabrication with the VARTM technique involved three main steps: mold preparation, filling with resin, and curing. First, the mold surface was treated with TR HIGH-TEMP mold release. The carbon fiber layers were stacked in the desired joint pattern. Then, the reinforcements were covered by a piece of peel ply on the top carbon fiber layer. Both the chemical agent and peel ply were applied so that the final composite joint fabric after curing could be released readily. An infusion mesh was applied over the peel ply, providing two main functions: promoting resin flow and facilitating the drawing of any voids before resin curing. Two rubber connectors and spiral tube pieces were placed as the inlet and vent for the mold. The whole package was enclosed in a vacuum bag and sealed with gum tape. Finally, two external hoses were connected to the inlet and vent. One was connected to the resin source and the other to a vacuum pump. To ensure a leakage-free mold, a sealing test was performed before resin filling. In this, the inlet was closed and the vacuum pump was turned on to draw the air trapped inside the mold. Then, the vent line was closed, the vacuum pump was switched off, and the

mold was left for 1 h. Next, the line was opened and any movement of the pressure gauge indicated leakage that needed to be addressed. After the resin had filled the mold and excess resin had exited the vent, the inlet was closed and the vent was left open for 24 h until the resin had cured. All VARTM processes were performed at room temperature

Testing procedure

The CFRP joints were sectioned to form specimens for the three-point bending tests, with the geometry shown in Figure 4. Five specimens were prepared for each condition. During the test, the specimen was monitored with AE measurements. The bending tests were carried out with a universal testing machine (Zwick 250, testXpert, ver. 11.02) at room temperature with a crosshead rate of 3 mm/min. Fracture processes were examined in real time using two AE sensors (micro30, Physical Acoustic Corp.), marked as S1 and S2, which were attached to the bending specimens using vacuum grease and mechanical fixation. The distance between the sensors and the load point was 23±1 mm (Fig. 4b). A two-channel AE detection system (MSTRAS 2001, Physical Acoustic Corp.) was used to record the AE data, and the AE measurement conditions included a 40-dB pre-amp, a threshold level of 40 dB, and a sampling rate of 4 MHz. A band-pass filter (range, 1 kHz to 1 MHz) under software control was used for signal gain for specific frequencies. Three AE parameters were investigated: amplitude, energy, and the frequency spectrum of the AE signals, obtained using an FFT. AE analysis can provide a way to identify and differentiate fracture sources. Consistent with Yoon et al. [30], we assumed that the distance between the sensor and the crack was sufficient to measure the AE characteristics. Considering the attenuation problems at high frequencies, we focused primarily on frequency bands below 400 kHz for verification of the fracture mechanism. Fractographic analyses were also performed on the fracture surface of the test specimens using optical microscopy and scanning electron microscopy (SEM). The fractographic results were used for quantitative and qualitative analyses.

Results and discussion

Table 3 shows thickness data obtained for the NCLJ. The average thicknesses were 1.83 and 3.08 mm for 6 and 10 layers, respectively. The minimum thickness and % max thickness deviation were recorded as measures of product quality. Table 1 shows that the minimum thicknesses were 1.78 and 2.932 mm for 6 and 10 layers, respectively. Furthermore, the % max thickness deviation ranged from 5% for 6 layers to 10% for 10 layers.

For the SCLJ, Table 2 shows that the average thicknesses for 5 and 7 carbon fiber layers were 1.34 and 1.81 mm, respectively. The minimum thicknesses were 1.15 and 1.55 mm for 5 and 7 layers, respectively. However, the % max thickness deviation was as high as 30%. The minimum thickness and % max thickness deviation indicated the degree of local thinning for the SCLJ.

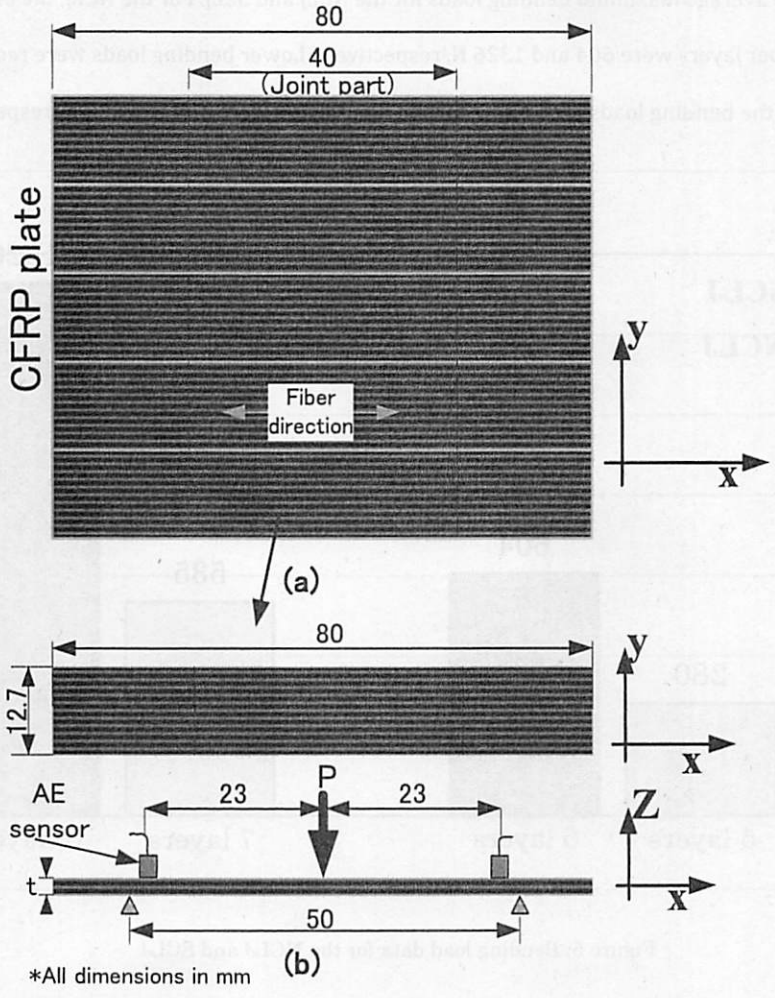

Figure 4: Specimen preparation. (a) Location of specimens taken from the CFRP plate and (b) an illustration of the specimen for the three-point bending testing with acoustic emission (AE) monitoring.

Table 1: Thickness measurements for the NCLJ

	Thickness, mm	minimum thickness, mm	% max thickness deviation
6 layers	1.83(0.04)	1.78	5
10 layers	3.08(0.12)	2.932	10

Table 2: Thickness measurements for the SCLJ

	Thickness, mm	minimum thickness, mm	% max thickness deviation
5 layers	1.34(0.18)	1.15	29
7 layers	1.81(0.25)	1.55	31

Figure 5 shows the average maximum bending loads for the NCLJ and SCLJ. For the NCLJ, the bending loads for 6 and 10 carbon fiber layers were 604 and 1326 N, respectively. Lower bending loads were recorded for the SCLJ. For example, the bending loads for 5 and 7 carbon fiber layers were 280 and 535 N, respectively.

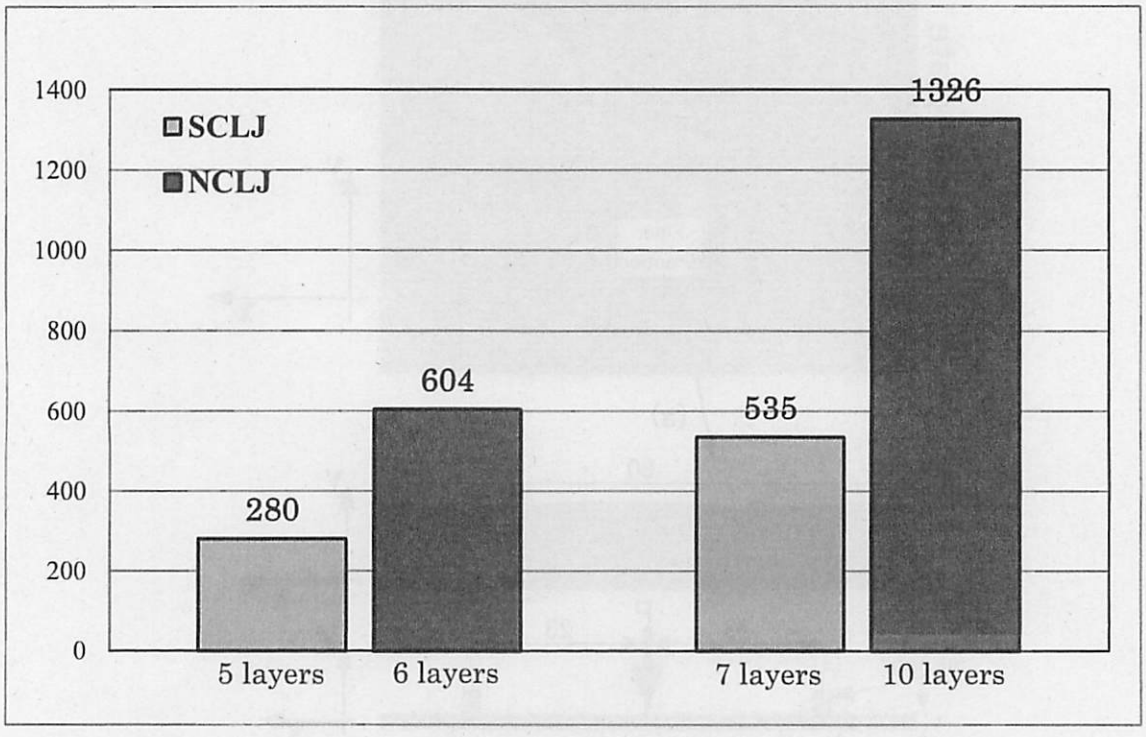

Figure 5: Bending load data for the NCLJ and SCLJ

The bending strength was markedly affected by the placement of carbon fiber layers. This behavior can be examined using AE, optical microscopy, and SEM techniques. Figures 6a-b and 7a-b show typical three-point bending stress behaviors with accompanying amplitude distributions of the AE signals as functions of time for the NCLJ and SCLJ, respectively. For NCLJ, the bending strength, σ1, is given by:

$$\sigma_1 = 3PL/2Wt^2, \qquad (1)$$

where P is the maximum load point on the load-deflection curve, L is the span length, W is the specimen width, and t is the specimen thickness. For SCLJ, the bending strength of a specimen, σ2, is given by:

$$\sigma_2 = 3Pb/Wt_c^2, \qquad (2)$$

where b is the distance between the specimen end and the thinner section, and tc is the thickness of the specimen at the thinner section.

In Figures 6a-b and 7a-b, the stress behavior can be separated into two stages. In the first, the stress increased until the peak, along with few AE pulses. After reaching the peak, extensive amplitude pulses were generated with the stress drop-down. For NCLJ, the 6-layer joint reached a maximum stress level of 1200 MPa and generated amplitude pulses of 83 dB. Furthermore, there were a few high-amplitude pulses of 90 dB, followed with a sudden stress drop to 600 MPa. The NCLJ with 10 layers reached a higher maximum stress of 2000 MPa. After that, the stress decreased gradually to 1500 MPa, emitting large AE amplitude pulses of 95 dB.

SCLJs with 5 and 7 layers showed similar stress and AE patterns to the NCLJ with 6 layers. In this case, stress was calculated based on the minimum thickness using Eq. (2).

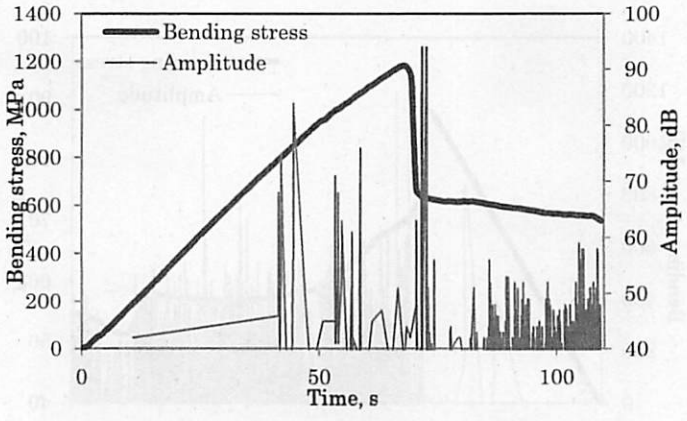

(a)

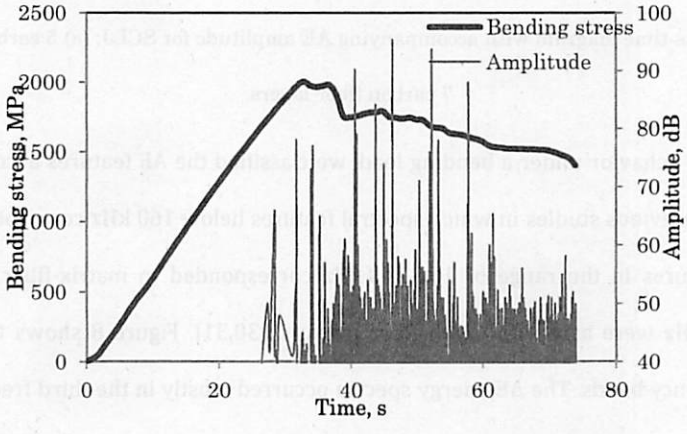

(b)

Figure 6: Bending stress-time diagram with accompanying AE amplitude for NCLJ: (a) 6 carbon fiber layers and (b) 10 carbon fiber layers

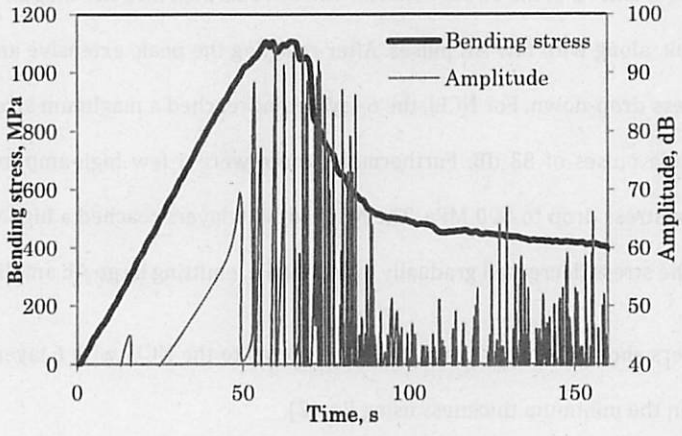

(a)

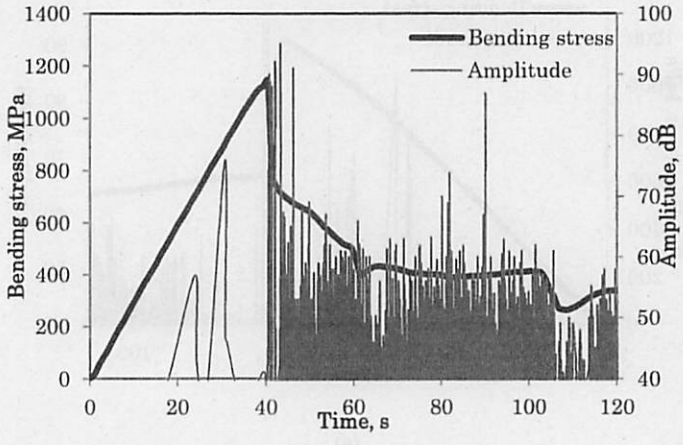

(b)

Figure 7: Bending stress-time diagram with accompanying AE amplitude for SCLJ: (a) 5 carbon fiber layers and (b) 7 carbon fiber layers.

To clarify the fracture behavior under a bending load, we classified the AE features according to the fracture mode on the basis of previous studies in which spectral features below 160 kHz corresponded to resin matrix fracture, spectral features in the range of 160-240 kHz corresponded to matrix-fiber mixed fracture, and features above 240 kHz were associated with fiber fracture [30,31]. Figure 8 shows the percentage of AE energy at these frequency bands. The AE energy spectra occurred mostly in the third frequency band ($f > 240$ kHz). The percentage of AE energy ranged from 85% for the NCLJ with 10 layers to 90% for 6 layers. Thus, the predominant fracture mode in the tests was fiber fracture.

To confirm the failure behavior of NCLJs, additional failure analyses using optical microscopy and SEM were performed. Figure 9 shows typical optical micrographs and an SE micrograph of the NCLJ with 10 layers. A bending fracture occurred at the center of the specimen, not at the joint ends. This indicated that the joining efficiency was at least 80% because, at the same bending load, the bending stress at the joint ends approximated 80% of the bending stress at the middle of the specimen.

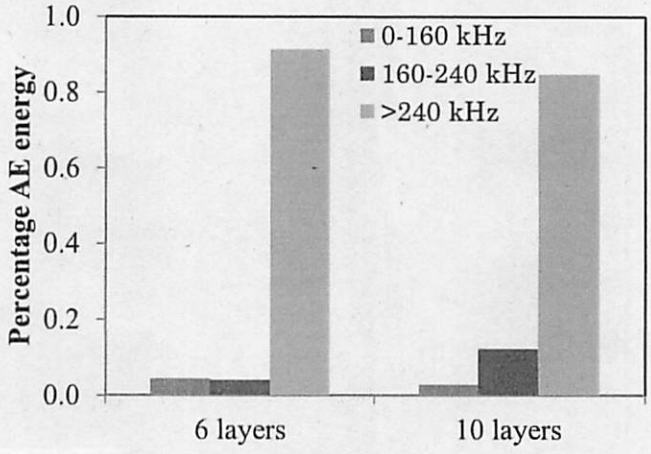

Figure 8: Typical percentage AE energy data for the three frequency bands for NCLJ.

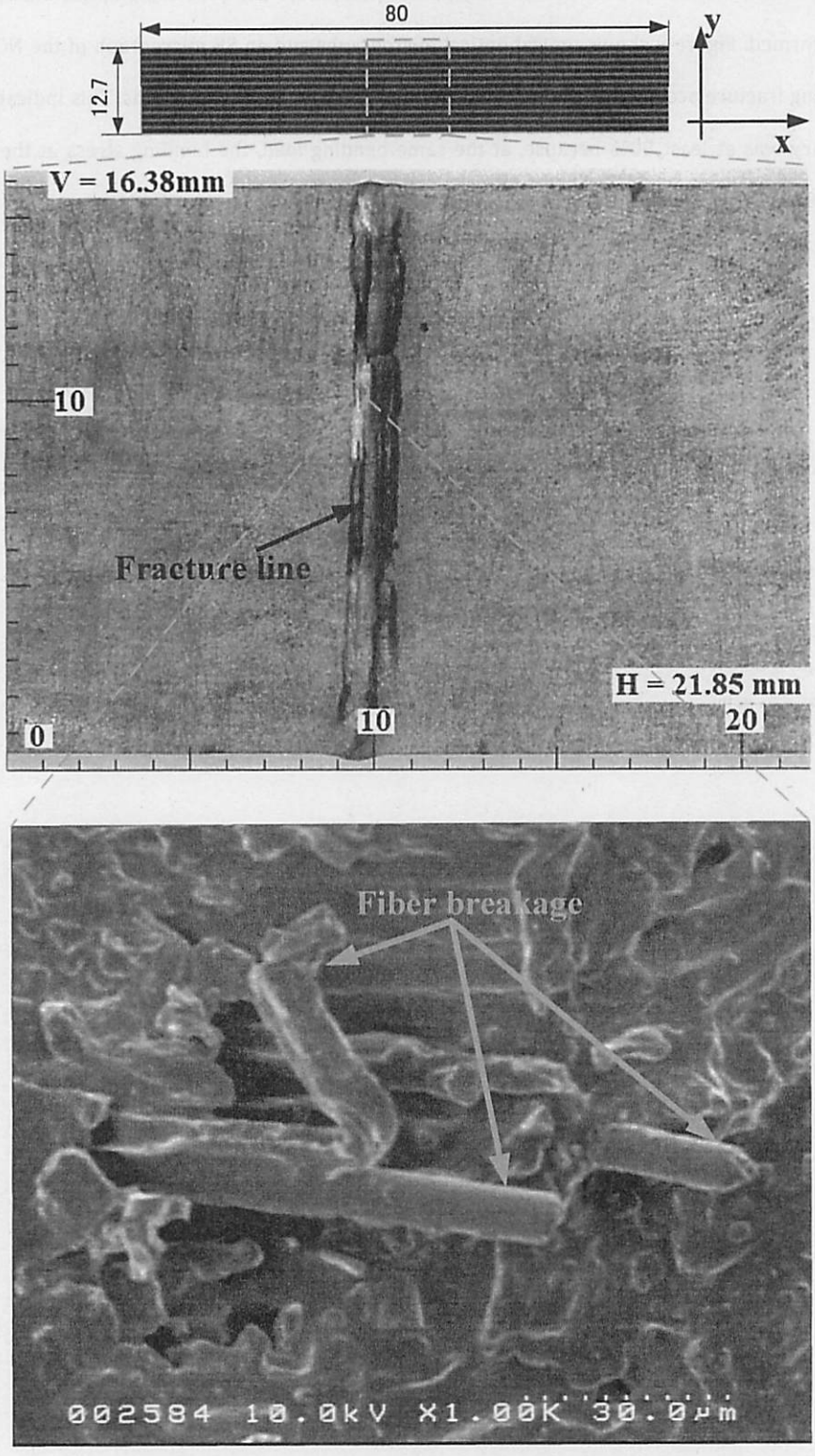

Figure 9: Typical optical microscopy and SEM micrographs for the fracture of NCLJ with 10 layers.

In contrast, AE and SEM analyses for the SCLJ showed different failure behavior. Figure 10 shows the percentage of AE energy at the adopted frequency bands for the SCLJ. A higher fraction of the AE energy spectrum occurred in the first frequency band (f < 160 kHz). This indicated that the fracture occurred due to resin failure. This behavior was confirmed by optical microscopy, as shown in Figure 11. For the SCLJ with 5 layers, a crack was initiated at the joint end and then propagated at the laminate interface until the final rupture.

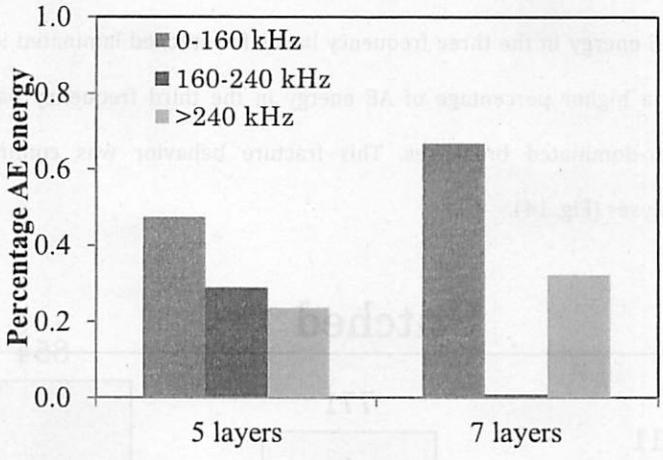

Figure 10: Typical percentage AE energy data for the three frequency bands for SCLJ.

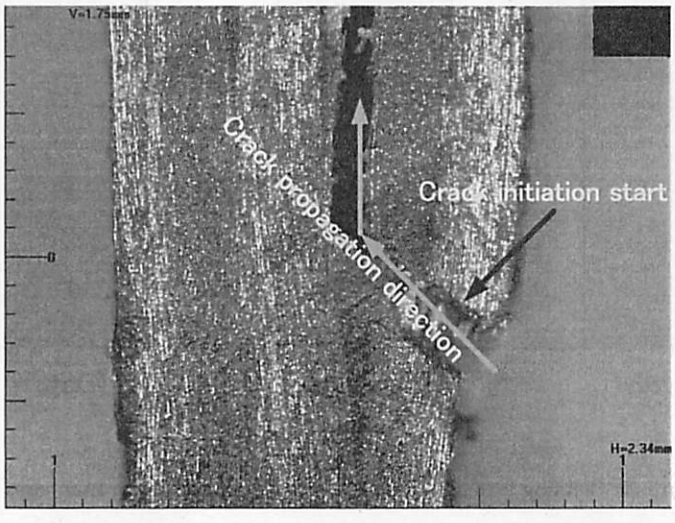

Figure 11: Typical optical micrographs for the fracture of the 5-layer SCLJ

For the second joint, the stitched laminated joint, an improved bending load resulted versus the conventional laminated joint. The bending load for an SLJ with 6 layers was 771 N. This represents a considerable increase, 27%, over the conventional laminated joint (Fig. 12). Plain and Tong [32] used a stitching technique to

improve mode I and II fracture toughness for laminated composites. Velmurugan et al. [33] showed retarded crack initiation, followed by gradual crack propagation, when stitching was applied to a cylindrical shell subjected to axial compression. For bending, Chung et al. [34] found that the stitching improved the strength of CFRP and KFRP composites under 4-point bending, by ~25%. Adanur and Tsao [35] reported an improvement in the flexural properties of KFRP and CFRP even when stitched at a comparatively low density. However, at higher stitch densities, the properties deteriorated.

Stitched laminated joints were analyzed by AE, optical microscopy, and SEM. Figure 13 shows typical percentages of AE energy in the three frequency bands for stitched laminated joints with 5, 6, and 7 layers. The SLJ showed a higher percentage of AE energy in the third frequency band (> 240 kHz). This behavior indicated fiber-dominated breakages. This fracture behavior was confirmed by the optical microscopy and SEM analyses (Fig. 14).

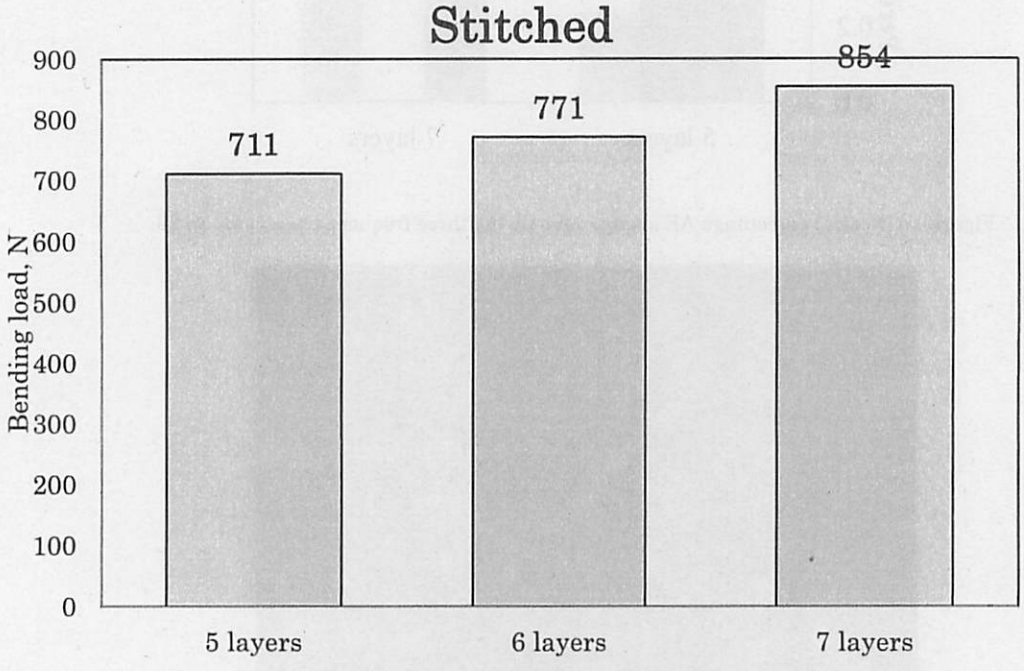

Figure 12: Bending load data for the SLJ with different layer numbers.

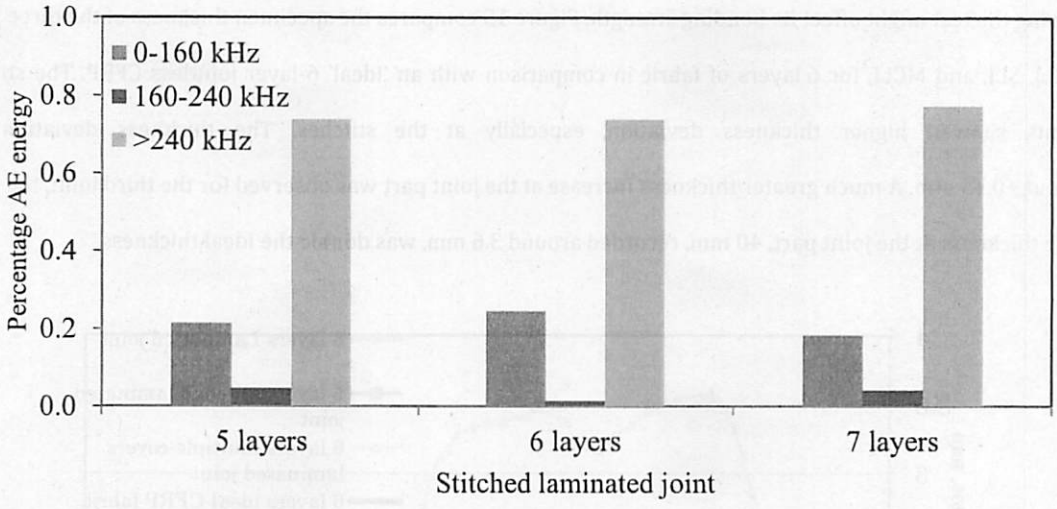

Figure 13: Typical percentage AE energy data for the three frequency bands for SLJ.

Figure 14: Typical SEM micrograph for the fracture of the 6-layer SCLJ.

For the third joint type, the multiple-cover laminated joint, a greater thickness for the joint part than for the adherend was observed. This joint was characterized by extra inserted carbon fiber pieces. The number of additional carbon fiber pieces exceeded the number of carbon fiber layers for the adherend. Thus, the thickness at the joint part should be at least twice the thickness of the adherend. This thickness difference occurred in the specimen length direction because all carbon fibers, including the additional carbon fiber pieces, were placed on a rigid flat surface of the mold (Fig. 2d). Thus, a thickness difference was observed at the upper surface of the joint in contact with the flexible vacuum bag. The positioning of this joint specimen

during the test might affect its bending strength. Figure 15 compares the specimen thickness of the three joints, NCLJ, SLJ, and MCLJ, for 6 layers of fabric in comparison with an 'ideal' 6-layer jointless CFRP. The stitched joints showed higher thickness deviation, especially at the stitches. The thickness deviation was about +0.45 mm. A much greater thickness increase at the joint part was observed for the third joint, the MCLJ. The thickness at the joint part, 40 mm, recorded around 3.6 mm, was double the ideal thickness.

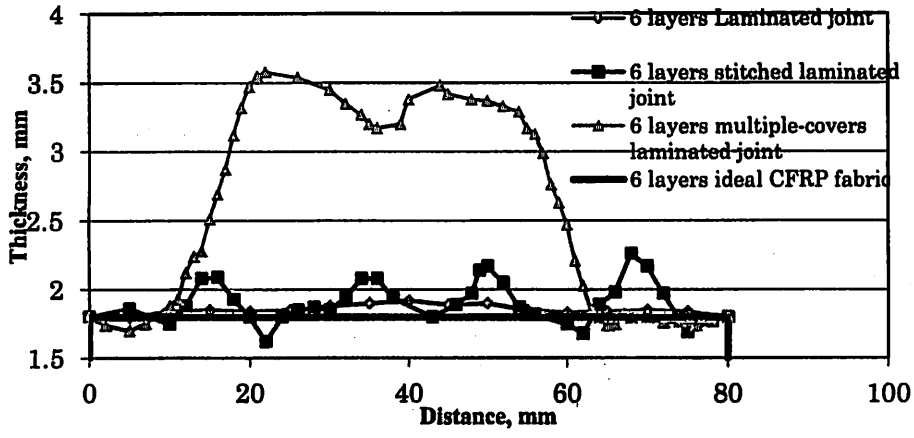

Figure 15: Typical thickness profiles for the three joints and the jointless CFRP fabric.

For the bending test results, the MCLJ achieved much higher bending loads than the conventional laminated joint and the stitched laminated joints. For example, the MCLJ with 6 layers showed a bending load of 1280 N, representing increases of 112% and 66% versus conventional laminated and stitched laminated joints. The MCLJ with 10 layers achieved 1958 N, an increase of 58% (Fig. 16).

Similar to the SLJ, the MCLJ showed dominant fiber breakage, as confirmed in the percentage AE energy in the third frequency band, > 240 kHz (Fig. 17), and many broken fibers on the surface (Fig. 18).

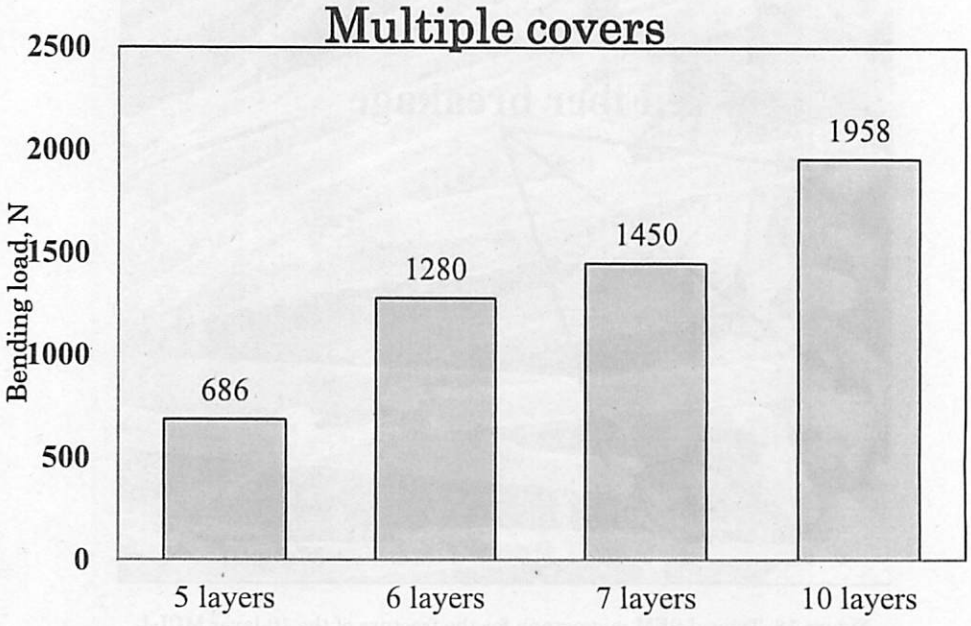

Figure 16: Bending load data for the MCLJ with different layer numbers.

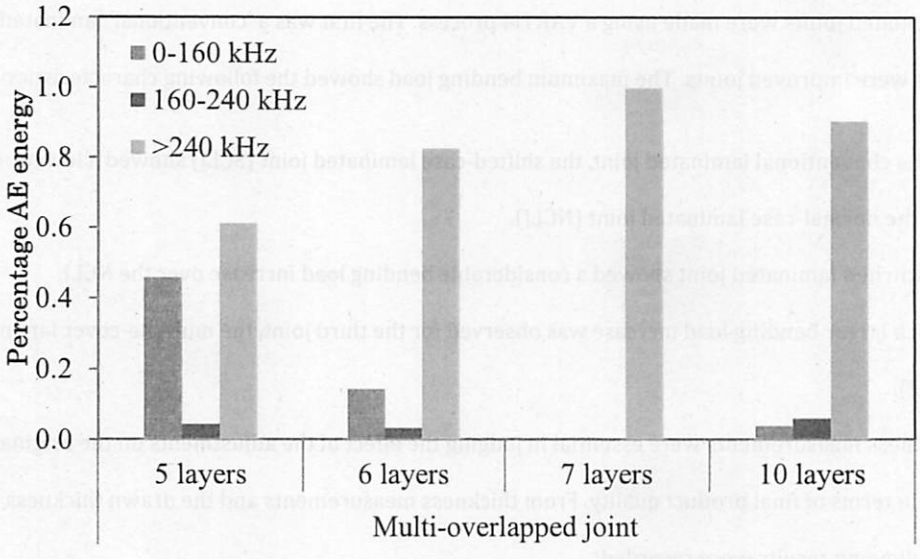

Figure 17: Typical percentage AE energy data for the three frequency bands for MCLJ.

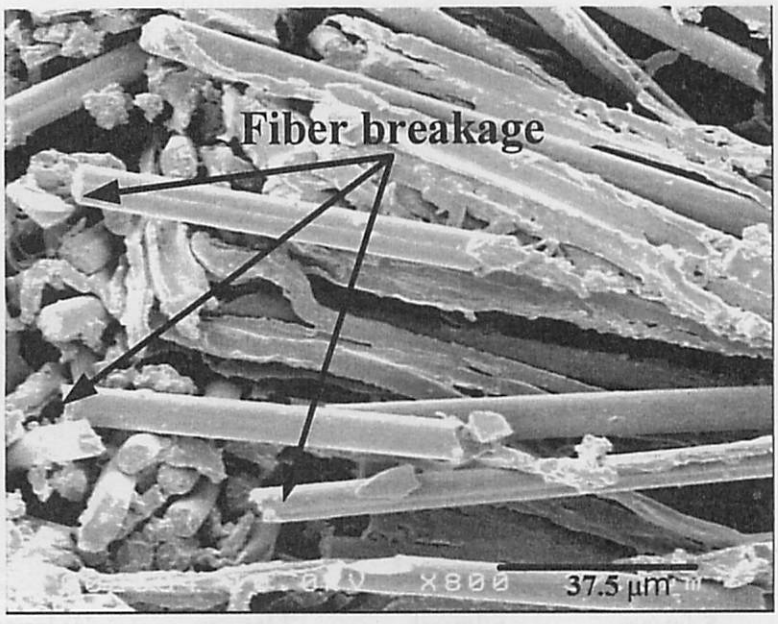

Figure 18: Typical SEM micrograph for the fracture of the 10-layer MCLJ.

Conclusions

Three laminated joints were made using a VARTM process. The first was a 'conventional' laminated joint and the others were improved joints. The maximum bending load showed the following characteristics:

1- For the conventional laminated joint, the shifted-case laminated joint (SCLJ) showed a lower bending load than the normal-case laminated joint (NCLJ).

2- The stitched laminated joint showed a considerable bending load increase over the NCLJ.

3- A much larger bending load increase was observed for the third joint, the multiple-cover laminated joint (MCLJ).

4- Thickness measurements were essential in judging the effect of the adjustments on the original laminated joint in terms of final product quality. From thickness measurements and the drawn thickness profiles, the following results were recorded:

5- Failure analysis for the three joints was performed using in-line AE monitoring as well as fracture surface observations. Resin failure was prevalent for the SCLJ, while fiber breakage was dominant for the NCLJ. However, with any movement in the carbon fiber layers, such as in the SCLJ, the failure mode changed to resin failure, rather than fiber breakage, causing lower bending strength. Both failure behaviors, fiber and resin failures, were confirmed using post-failure analyses. Fiber breakage was dominant for the two other joint types, SLJ and MCLJ.

ACKNOWLEDGMENT

This work was partly supported by a research grant from the Japan Society for Promotion of Science (#26630496), and by the Collaborative Research Program of Research Institute for Applied Mechanics, Kyushu University.

References

[1]. Falconieri, D., & Franco, F. (2015). The effect of titanium insert repairs on the static strength of CFRP coupons and joints. Composite Structures, 134, 799–810. doi:10.1016/j.compstruct.2015.08.042

[2]. Weinzierl, M., Schatz, M., Antonelli, V., & Baier, H. (2016). Structural design optimization of CFRP chopper disks. Composite Structures, 140, 351–359. doi:10.1016/j.compstruct.2015.12.016

[3]. Ou, Y., Zhu, D., Zhang, H., Yao, Y., Mobasher, B., & Huang, L. (2016). Mechanical properties and failure characteristics of CFRP under intermediate strain rates and varying temperatures. Composites Part B: Engineering, 95, 123–136. doi:10.1016/j.compositesb.2016.03.085

[4]. Lang, H., Nogueira, A. C., Jürgens, M., Hombergsmeier, E., Hinterhölzl, R., & Drechsler, K. (2016). Investigation on the structural behavior of a metallically 3D-reinforced CFRP/CFRP joint using a variable search based on finite element analyzes. Composite Structures, 139, 199–209. doi:10.1016/j.compstruct.2015.11.040

[5]. Dvorak, G. J., Zhang, J., & Canyurt, O. (2001). Adhesive tongue-and-groove joints for thick composite laminates. Composites Science and Technology, 61(8), 1123–1142. doi:10.1016/S0266-3538(01)00012-4

[6]. Abusrea, M. R., & Arakawa, K. (2016). Improvement of an adhesive joint constructed from carbon fiber-reinforced plastic and dry carbon fiber laminates. Composites Part B: Engineering, 97, 368–373. doi:10.1016/j.compositesb.2016.05.005

[7]. Padhi, G. ., McCarthy, M. ., & McCarthy, C. . (2002). BOLJAT: a tool for designing composite bolted joints using three-dimensional finite element analysis. Composites Part A: Applied Science and Manufacturing, 33(11), 1573–1584. doi:10.1016/S1359-835X(02)00113-6

[8]. Ueda, M., Miyake, S., Hasegawa, H., & Hirano, Y. (2012). Instantaneous mechanical fastening of quasi-isotropic CFRP laminates by a self-piercing rivet. Composite Structures, 94(11), 3388–3393. doi:10.1016/j.compstruct.2012.04.027

[9]. Thoppul, S. D., Finegan, J., & Gibson, R. F. (2009). Mechanics of mechanically fastened joints in polymer–matrix composite structures – A review. Composites Science and Technology, 69(3-4), 301–329. doi:10.1016/j.compscitech.2008.09.037

[10]. Friedrich, C., & Hubbertz, H. (2014). Friction behavior and preload relaxation of fastening systems with composite structures. Composite Structures, 110, 335–341. doi:10.1016/j.compstruct.2013.11.024

[11]. Lee, Y.-H., Lim, D.-W., Choi, J.-H., Kweon, J.-H., & Yoon, M.-K. (2010). Failure load evaluation and prediction of hybrid composite double lap joints. Composite Structures, 92(12), 2916–2926. doi:10.1016/j.compstruct.2010.05.002

[12]. Oplinger JW. Mechanical fastening and adhesive bonding. In: Peters ST, editor. Handbook of composites. New York: Springer; 1998.

[13]. Abusrea, M., R., Jiang, S., Chen, D., Arakawa, K., . Novel CFRP Adhesive Joints and Structures for Offshore Application. International Journal of Chemical, Molecular, Nuclear, Materials and Metallurgical Engineering 9 (9), 2015

[14]. Chen, D., Arakawa, K., Jiang, S., . Novel joints developed from partially un-moulded carbon-fibre-reinforced laminates. Journal of Composite Materials, 2015, Vol. 49(14) 1777–1786.

[15]. Ascione, F. (2016). The influence of adhesion defects on the collapse of FRP adhesive joints. Composites Part B: Engineering, 87, 291–298. doi:10.1016/j.compositesb.2015.10.033

[16]. Rahman, N. M., & Sun, C. T. (2014). Strength calculation of composite single lap joints with Fiber-Tear-Failure. Composites Part B: Engineering, 62, 249–255. doi:10.1016/j.compositesb.2014.03.004

[17]. de Castro, J., & Keller, T. (2008). Ductile double-lap joints from brittle GFRP laminates and ductile adhesives, Part I: Experimental investigation. Composites Part B: Engineering, 39(2), 271–281. doi:10.1016/j.compositesb.2007.02.015

[18]. Heim, D., Hartmann, M., Neumayer, J., Klotz, C., Ahmet-Tsaous, Ö., Zaremba, S., & Drechsler, K. (2013). Novel method for determination of critical fiber length in short fiber carbon/carbon composites by double lap joint. Composites Part B: Engineering, 54, 365–370. doi:10.1016/j.compositesb.2013.05.026

[19]. Hart-Smith LJ. Further developments in the design and analysis of adhesively bonded structural joints. Joining of Composite Materials, ASTM STP 1981;749:3–31.

[20]. Salih Akpinar. The strength of the adhesively bonded step-lap joints for different step numbers. Composites: Part B 67 (2014) 170–178 doi:10.1016/j.compositesb.2014.06.023

[21]. Löbel, T., Kolesnikov, B., Scheffler, S., Stahl, a., & Hühne, C. (2013). Enhanced tensile strength of composite joints by using staple-like pins: Working principles and experimental validation. Composite Structures, 106, 453–460. doi:10.1016/j.compstruct.2013.06.020

[22]. Mouritz AP, Chang P, Cox BN. Fatigue properties of z-pinned aircraft composite materials. ICAS Int Cong Aeronaut Sci 2006.

[23]. Dransfield, K. A., Jain, L. K., & Mai, Y.-W. (1998). On the effects of stitching in CFRPs—I. mode I delamination toughness. Composites Science and Technology, 58(6), 815–827. doi:10.1016/S0266-3538(97)00229-7

[24]. Heß, H., & Himmel, N. (2011). Structurally stitched NCF CFRP laminates. Part 1: Experimental characterization of in-plane and out-of-plane properties. Composites Science and Technology, 71(5), 549–568. doi:10.1016/j.compscitech.2010.11.012

[25]. Kim, J. H., Park, B. J., & Han, Y. W. (2004). Evaluation of fatigue characteristics for adhesively-bonded composite stepped lap joint. Composite Structures, 66(1), 69–75. doi:10.1016/j.compstruct.2004.04.023

[26]. Abe K-i, Ohya Y. An investigation of flow fields around flanged diffusers using CFD. Journal of Wind Engineering and Industrial Aerodynamics. 2004;92(3–4):315-330.

[27]. Abe K, Nishida M, Sakurai A, Ohya Y, Kihara H, Wada E, et al. Experimental and numerical investigations of flow fields behind a small wind turbine with a flanged diffuser. Journal of Wind Engineering and Industrial Aerodynamics. 2005;93(12):951-970.

[28]. Ohya Y, Karasudani T. A Shrouded Wind Turbine Generating High Output Power with Wind-lens Technology. Energies. 2010;3(4):634-649.

[29]. Abusrea, M., R., and Arakawa, K., Evaluation of the strength of CFRP adhesive joints manufactured using VARTM. 10th International Symposium on Advanced Science and Technology in Experimental Mechanics, November 1-4, 2015, Matsue, Japan

[30]. Yoon, SY., Arakawa K., Han, SW., Chen, D., and Choi, NS.,. Effect of Compaction Treatment on Laminated CFRP Composites Fabricated by Vacuum-Assisted Resin-Transfer Molding. 2015; DOI:10.1002/pc.23578

[31]. Gu, J.-U., Yoon, H.-S., & Choi, N.-S. (2012). Acoustic emission characterization of a notched aluminum plate repaired with a fiber composite patch. Composites Part A: Applied Science and Manufacturing, 43(12), 2211–2220. doi:10.1016/j.compositesa.2012.07.018

[32]. Plain, K. P., & Tong, L. (2011). An experimental study on mode I and II fracture toughness of laminates stitched with a one-sided stitching technique. Composites Part A: Applied Science and Manufacturing, 42(2), 203–210. doi:10.1016/j.compositesa.2010.11.006

[33]. Velmurugan, R., Gupta, N. K., Solaimurugan, S., & Elayaperumal, A. (2004). The effect of stitching on FRP cylindrical shells under axial compression. International Journal of Impact Engineering, 30(8), 923–938. doi:10.1016/j.ijimpeng.2004.04.007

[34]. Chung, W. C., Jang, B. Z., Chang, T. C., Hwang, L. R., & Wilcox, R. C. (1989). Fracture behavior in stitched multidirectional composites. Materials Science and Engineering: A, 112, 157–173. doi:10.1016/0921-5093(89)90355-9

[35]. S. Adanur, Y.P. Tsao. Stitch bonded textile structural compositesProc. 26th Int. SAMPE Tech. Conf. (1994), pp. 25–34

国際化推進共同研究概要

No.15

タイトル: Mechanical properties of laminated CFRP composites under and after impact loadings

研究代表者: CHEN, Dingding

所内世話人: 新川 和夫

実施期間: 2016年11月24日 ～11月28日

研究概要: 真空樹脂含浸法を応用することにより炭素繊維強化複合材料(CFRP)を作製し、CFRPの内部に接続部分を導入すると、引張り強度が低下することを示した。これは接続部の応力集中が初期き裂を発生させ、さらに異なる積層間に全体破壊を引き起こすことが原因である。したがって接続部分近傍のせん断応力と引張り応力が重要な役割を果たすこと、また接合部の強度向上には対象性を有する接合設計が必要となることを明らかにした。

Tensile properties of FRP ply splice structures

CHEN Dingding
College of Basic Education, NationalUniversity of Defense Technology, Changsha, China

Abstract: When the FRP structure becomes large, it is required to splice two or more plies to meet the size requirement. In order to understand the mechanical property of the FRP ply splice structure and get strong ply splice structures, the tensile properties of three kinds of unidirectional CFRP ply splice structures were tested. The tensile specimens were monitored during the loading process to analyze the fracture process, and FEM analysis was used to study the character of stress distributions when the ply splice structures are under a tensile load. All the CFRP materials were prepared through vacuum assisted resin transfer molding (VaRTM) process. The results show that, inducing ply splice into CFRP materials, the tensile strength decreases evidently. Due to the ply splice, stress concentration occurs, and the initial fracture happens in the ply splice position, leading to the final fracture on the interfaces between different plies. The interlaminar shear stress and the tensile stress in through-thickness direction near the ply splice position are the key factors leading to the initial failure. In order to get stronger ply splice structures, symmetric structure should be adopted.

Introduction

Due to high strength and low density, fiber reinforced plastics (FRP) have been used widely, and FRP structures with large size are required by more and more applications. When the FRP structure becomes large, only one reinforcement ply may not large enough. In this case, it is required to splice two or more plies (or fabrics) to meet the size requirement. The structure connecting two or more plies is called ply splice structure. The ply splice structure will play like a defect in a FRP structure and decrease the mechanical property. In order to use the FRP product with ply splice structures safely, it is necessary to master its mechanical properties. In this report, the tensile properties of three kinds of unidirectional CFRP ply splice structures were studied.

Experiments

Three kinds of CFRP plates with ply splice structures were made through vacuum assisted resin transfer molding (VaRTM) process. As shown in Fig. 1, the black line represents the unidirectional carbon fiber fabric. Four fabrics were adopted in each kind of specimens. The matrix is XNR/H6815 epoxy resin from Nagase. The fabrics are TENAX STS from Saeertex GmbH. The thickness of all the specimens is about 2 mm. The fiber volume content is about 55%.

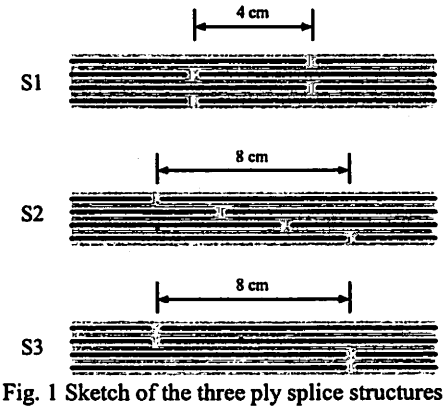

Fig. 1 Sketch of the three ply splice structures

Static tensile tests were performed to evaluate the three structures. The dimensions of the specimens are shown in Fig. 2; the length was 250mm and the width was 10 mm. Two pairs of tabs made with glass fiber-reinforced plastic were used for each specimen to reduce stress concentrations. The length of the tab was 50 mm. The crosshead speed was 1 mm/min. At least four samples were tested to get the average tensile strength. Additionally, the tensile strength along the fiber direction of a normal CFRP specimen with the same dimensions was tested as a reference.

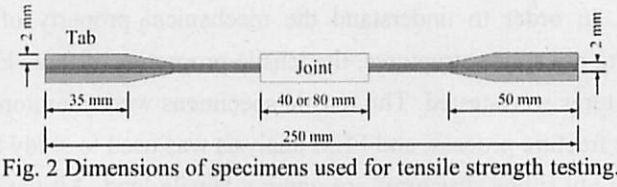

Fig. 2 Dimensions of specimens used for tensile strength testing.

Simulation

The stress state of the three ply splice structures under tensile loads were studied using FEM method. The model was simplified. Take S1 structure for example. As shown in Fig. 3, only the region where two plies were connected was set as the resin property. The other region was set as CFRP property.

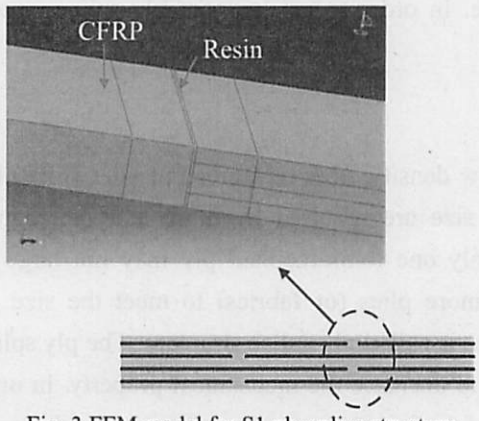

Fig. 3 FEM model for S1 ply splice structure

Results and discussion

Fig. 4 shows the tensile strength of the three ply splice structures and the normal CFRP material. The strength of all the ply splice structures was much lower than the normal CFRP. S1 and S2 have similar strength and are stronger than S3 structure. Figures 5-7 contain typical tensile load–displacement curves for the three ply splice structures. It can be found that, for all structures, crack initiation occurred at the region where the plies were connected. As the tensile load increased, the crack propagated, finally leading to the final fracture. All the fracture happened on the interlaminar surface. The crack initiation of S3 occurred earlier than S1 and S2.

Fig. 8 shows the distribution of tensile stress in through-thickness direction (S_{22}), shear stress and tensile stress along fiber direction (S_{11}) for the three structures under the tensile load of 14 kN. Due to the ply splice structure, serious stress concentration was induced. However, the stress concentration caused by one ply splice point was not affected by another ply splice point. Consequently, a deduction could be made that the strength of the three ply splice structures are decided by the stress concentration caused by each independent ply splice point.

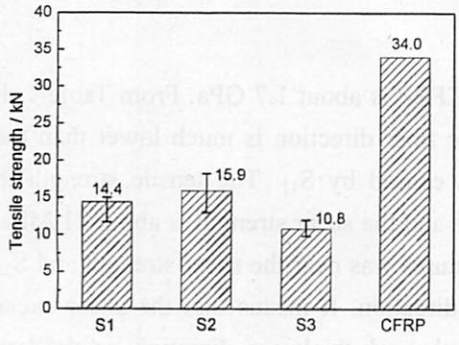

Fig. 4 Tensile strength of different ply splice structures and CFRP plate for 10 mm wide specimens

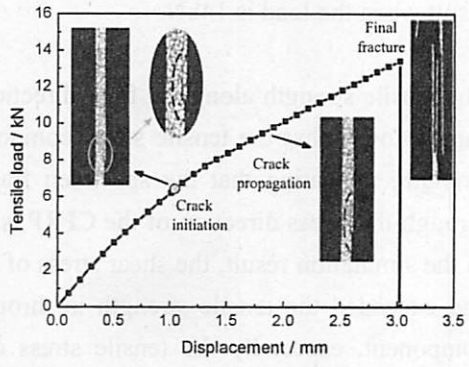

Fig. 5 Typical load-displacement curve for a S1 structure

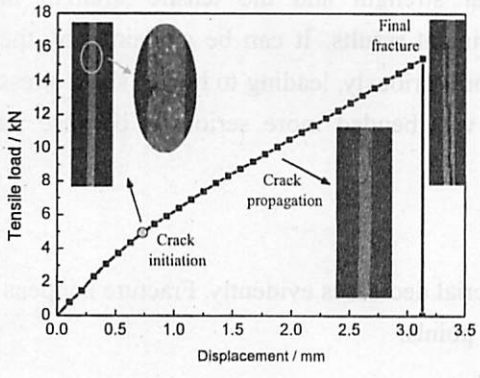

Fig. 6 Typical load-displacement curve for a S2 structure

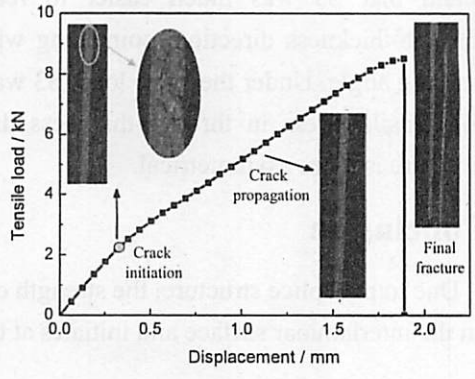

Fig. 7 Typical load-displacement curve for a S3 structure

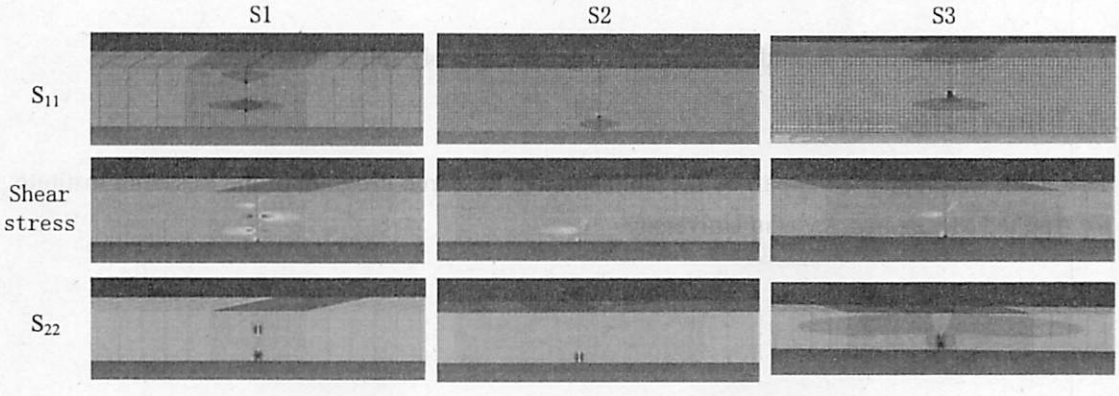

Fig. 8 Distribution of S_{11}, interlaminar shear stress and S_{22} in vicinity of ply splice position for the three types of structures

Table 1 List of the maximum value of stress when the load is 4kN and the bending angle when the load is 14kN

	S1	S2	S3
S_{11}/MPa	445	433	419
Shear stress/MPa	20.7	20.9	22.9
S_{22}/MPa	86.7	89.4	110.3
Bending angle /°	0.4	0.3	0.5

Table 1 lists the maximum value of stress when the load was 4kN. The simulation results were used to analyze the crack initiation of the structures. In experiments, for the three structures, crack

initiation occurred at about 4kN. In order to find the difference easier, the bending angle was the result when the load is 14kN.

The tensile strength along the fiber direction of normal CFRP is about 1.7 GPa. From Table 1, it can be found that the tensile stress component along the fiber direction is much lower than the strength, indicating that the specimen fracture was not caused by S_{11}. The tensile strength in through-thickness direction of the CFRP is about 72 MPa and the shear strength is about 21 MPa. In the simulation result, the shear stress of the three structures was near the shear strength and S_{22} had exceeded the tensile strength in through-thickness direction. It means that the shear stress component, especially the tensile stress component in through-thickness direction, is the key factor leading to the fracture.

Comparing the shear stress component and S_{22} component among the three structures, it can be found that S3 was much easier to reach the shear strength and the tensile strength in through-thickness direction, coinciding with the experiment results. It can be explained by the bending angle. Under the same load, S3 was bended more seriously, leading to higher shear stress and tensile stress in through-thickness direction. S3 was bended more seriously, because its structure is more asymmetrical.

Conclusion

1. Due to ply splice structure, the strength of CFRP material decreases evidently. Fracture happens on the interlaminar surface and initiates at the ply splice points.

2. The shear stress component and tensile stress component in through-thickness direction at the stress concentration area are the key factors leading the fracture.

3. Symmetric structures should be designed to get stronger ply splice structures.

Acknowledgements

This work was supported in part by the Collaborative Research Program of the Research Institute for Applied Mechanics, Kyushu University

国際化推進共同研究概要

No.16

タイトル: CFD prediction of unsteady aerodynamic and hydrodynamic performances of floating offshore wind turbine

研究代表者: WAN, Decheng

所内世話人: 胡 長洪

実施期間: 2017年1月21日 ～ 1月25日

研究概要: 国際化推進共同研究「CFD prediction of unsteady aerodynamic and hydrodynamic performances of floating offshore wind turbine」では今年度は2年目で，共同研究・研究集会とも予定通り実施した。研究集会について，世話人が担当したエネルギー基盤技術国際教育研究センターの研究集会と共同開催で，外国から9名，日本から約35名の参加者があり，海洋再生可能エネルギー開発に関する有意義な国際研究集会となった。

Report for 2016 RIAM International Joint Research Project

CFD prediction of unsteady aerodynamic and hydrodynamic performances of floating offshore wind turbine

Purpose

This two year project is aiming to accelerate the research on CFD simulation of floating offshore wind turbine (FOWT) flows which has already been carried out both at SJTU and RIAM. Through this interactional joint research project, (a) a useful database will be established for calibrations, validations & comparisons of different CFD codes on FOWT; (b) a better understanding of the hydrodynamic and aerodynamic behavior of offshore floating wind turbine will be expected. This joint research will also enhance the state-of-the-art scientific knowledge in a broad range of offshore engineering application. In addition the project will contribute to the technical training of graduate students for active participation in the multi/inter-disciplinary workforce of the future.

Research Plan

(1) Carry out collaborative research between SJTU and RIAM, in the area of advanced modeling of unsteady hydrodynamic and aerodynamic forces interacting on offshore floating wind turbine, to provide a benchmark for validation and comparison of various analytical, simulation and experimental models on the study of the floating offshore wind turbine problem.

(2) Evaluate the system's responses of 6DOF motions, which are excited by both wave and wind under various conditions as well as the rotation of blades.

(3) Organize an international symposium in the end of each fiscal year, in which relative researchers will present and discuss their research results

The members involved in this collaborative research are shown in the following table.

Researcher's Name	Name of University or Institute	Present Status or Grade (graduate students)	Researcher role
Decheng Wan	SJTU	Professor	Representative person (CFD)
Zhiqiang Hu	Newcastle University	Lecturer	Co-researcher (Experiment)
Ping Cheng	SJTU	PhD student	Co-researcher (CFD)
Yong Ai	SJTU	Graduate student	Co-researcher (CFD)
Makoto Sueyoshi	RIAM	Assistant professor	Co-researcher (experiment)
Cheng Liu	RIAM	Posdoc	Co-researcher (CFD)
Changhong Hu	RIAM	Professor	RIAM Attendant

Summary of Collaboration Research

In 2016, a coupling rotor-platform-mooring system solver, FOWT-UALM-SJTU, has been developed and applied to the NREL-5MW Baseline wind turbine with coupled periodic surge and pitch motions of its supporting platform. To analyze the effect of coupled surge and pitch motion, a simulation with periodic surge motion alone is added, in which case the periodic surge motion is the same as the surge component in the coupled-motion case. From the simulation, the time series of the unsteady thrust and power coefficients are obtained, together with the detailed information of the wake flow field. The coupled surge and pitch motion shows larger effect on both thrust and power coefficient. The average of both thrust coefficient and power coefficient in surge-motion alone cases show good agreement with those in literature. The vorticity distribution changes rapidly when the rotor moves periodically, and the differences of the gap distance of each two adjacent vortex tubes at each instantaneous moment are observed.

As a main event of this international joint research project, 'International RIAM Symposium on Ocean Renewable Energy Technologies and Related Fluid Dynamics Researches' was held on January 23-24, 2017. On the symposium, overseas scholars are invited to present their recent researches on ocean renewable energy development.

The research budget provided for this international joint research has been used to support part of the travel expenses of the following 3 scholars to attend the symposium.

1. Decheng Wan, Professor of Shanghai Jiao Tong University, China
2. Zhiqiang Hu, Lecturer, Newcastle University, UK
3. Xiaobo Chen, Director, Deepwater Technology Research Center, Bureau Veritas, France

This symposium was financially supported by Research Institute for Applied Mechanics and Research and Education Center for Advanced Energy Materials, Devices, and Systems.

The program of the symposium is as follows.

PROGRAM

Date: January 23-24, 2017
Place: W601, RIAM, Kyushu University

23 January (Monday)

13:00 - 13:10	***Opening Address*** **Changhong Hu**

Session 1 ***Chair:*** **Changhong Hu**

13:10 - 14:00	**Yuji Ohya** (Kyushu University) *Keynote Lecture* Introduction of Wind-Lens Technology and Its Application - Efficient Utilization of Wind, Water and Solar Energy -
14:00 - 14:40	**Jens N. Sørensen** (Technical University of Denmark, DK) *Invited Lecture* Assessment of the Potential of Massive Exploitation of Offshore Wind Power in Europe
14:40 - 15:20	**Ryo S. Amano** (University of Wisconsin-Milwaukee, USA) *Invited Lecture* Wind and Hydro Energy
15:20 - 15:30	Coffee break

Session 2 ***Chair:*** **Decheng Wan**

15:30 - 16:10	**Jiahn-Horng Chen** (National Taiwan Ocean University, Taiwan, R.O.C.) *Invited Lecture* The System Dynamics of Floating Kuroshio Turbine System
16:10 - 16:40	**Yusaku Kyozuka, Patxi Garcia Novo** (Nagasaki University) Characteristics of Turbulence Intensity of Tidal Current in Goto Islands, Nagasaki
16:40 - 17:10	**Cheng Liu, Changhong Hu** (Kyushu University) CFD Simulation of a Tidal Turbine Farm by Using ACL Model
17:10 - 17:40	**Masashi Kashiwagi, Mariko Miki** (Osaka University) Realization of Cloaking and Wave-energy Absorption with Multiple Floating Bodies
18:00 – 21:00	Dinner Party

24 January (Tuesday)

Session 3 ***Chair:*** **Shigeo Yoshida**

9:10 - 9:50	**Decheng Wan** (Shanghai Jiao Tong University, China) *Invited Lecture* CFD Study of Aero- and Hydro- Dynamic Performances of Floating Offshore Wind Turbine
9:50 - 10:30	**Xiaobo Chen** (Bureau Veritas, France) *Invited Lecture* Some Special Aspects of TLP Windmill Concept
10:30 - 11:00	**Dief Tarek** (Kyushu University) Airborne Wind Energy
11:00 - 11:30	**Zhiqiang Hu** (Newcastle University, UK) A Program for Integrated Dynamic Characteristic Analysis of Floating Wind Turbine
11:30 - 12:00	**Makoto Sueyoshi** (Kyushu University) Wake Measurement of a Horizontal Axis Tidal Turbine
12:00 - 13:00	Lunch

Session 4 ***Chair:*** **Ching-Yeh Hsin**

13:00 - 13:40	**P. Ferrant, M. Gouin, G. Ducrozet** (LHEEA Lab, Ecole Centrale de Nantes, France) *Invited Lecture* Deterministic Simulation of Nonlinear Waves including Bathymetry Effects, with Applications to Naval and Offshore Engineering
13:40 - 14:20	**Yonghwan Kim** (Seoul National University, Korea) *Invited Lecture* Extreme Statistical Approach for the Second-Order Hydrodynamics of Offshore Structures
14:20 - 14:50	**Hiroshi Isshiki** (Inst. of Mathematical Analysis) On the Space-Time Integral Representation Method for Initial-Boundary Value Problem of Advective Diffusion
14:50 - 15:20	**Katsutoshi Shirasawa** (Okinawa Institute of Science and Technology) Development of an Ocean-Current Turbine at OIST
15:20 - 15:50	**Yuma Ito, Hidetsugu Iwashita** (Hiroshima University) Characteristics of Steady Aerodynamics of the Canard-Configuration WIG Flying in the Ground Effect
15:50 - 16:00	***Closing Address*** **Yuji Ohya**

国際化推進共同研究「CFD prediction of unsteady aerodynamic and hydrodynamic performances of floating offshore wind turbine」では今年度は２年目で，共同研究・研究集会とも予定通り実施した。研究集会について，世話人が担当したエネルギー基盤技術国際教育研究センターの研究集会と共同開催で，外国から９名，日本から約３５名の参加者があり，海洋再生可能エネルギー開発に関する有意義な国際研究集会となった。

国際化推進共同研究概要

No.17

タ イ ト ル: Study of dislocation generation in silicon ribbons: comparison between 2D and 3D crystal growth dynamics

研究代表者: SERRA, JOAO, MANUEL

所内世話人: 柿本 浩一

実 施 期 間: 2016 年 8 月 5 日 ～8 月 13 日

研究概要: :新規シリコン溶融法を用いて、太陽電池用のシート結晶を作成した。この結晶をＸ線回折法により、結晶欠陥の評価を行った。その結果、転位が導入されており、今後共同研究で、無転位化に向けた結晶成長条件等の探索を行い、無転位シリコン結晶シートの作成を行う。

Report on the visit to Japan during the ICCGE-18 Conference

Study of dislocation generation in silicon ribbons: comparison between 2D and 3D crystal growth dynamics

J.M. Serra, University of Lisbon, Portugal and K.Kakimoto, Kyushu University, Japan

Joint research: project nº17 on Renewable Energy Dynamics

Date: August 7th - 12th, 2016.

The purpose of this mission was to present results about the crystallization of silicon ribbons in the framework of a collaboration work between the University of Lisbon, Portugal and Kyushu University, Japan during the International Conference on Crystal Growth and Epitaxy.

The mission comprised:

- Presentation of the research activities of the group of the University of Lisbon related to crystal growth for photovoltaic applications

- Meetings with Dr. Nakano to discuss scientific issues

- Deliver some silicon crystallized material to be characterized by Prof. Kakimoto team in Kyushu

Some results of the characterization of those silicon ribbons are indicated below

Sample: 2mm/min

Diffraction 220 →

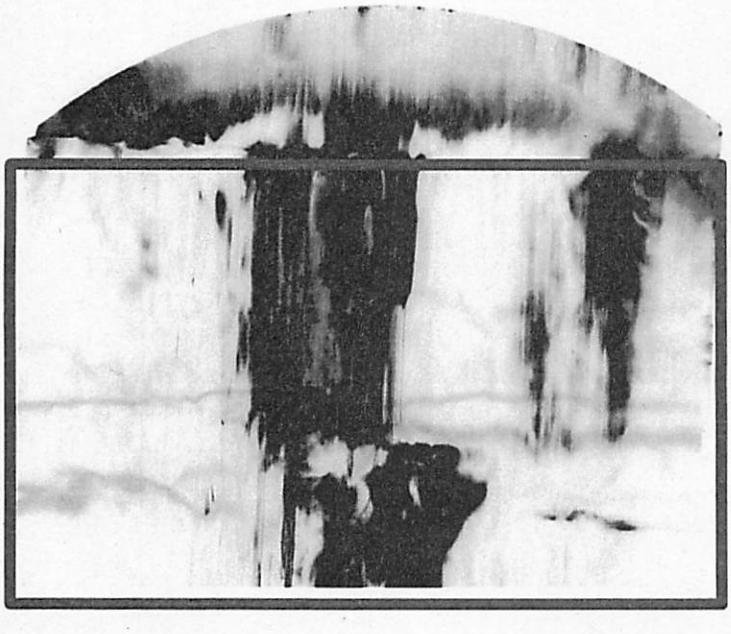

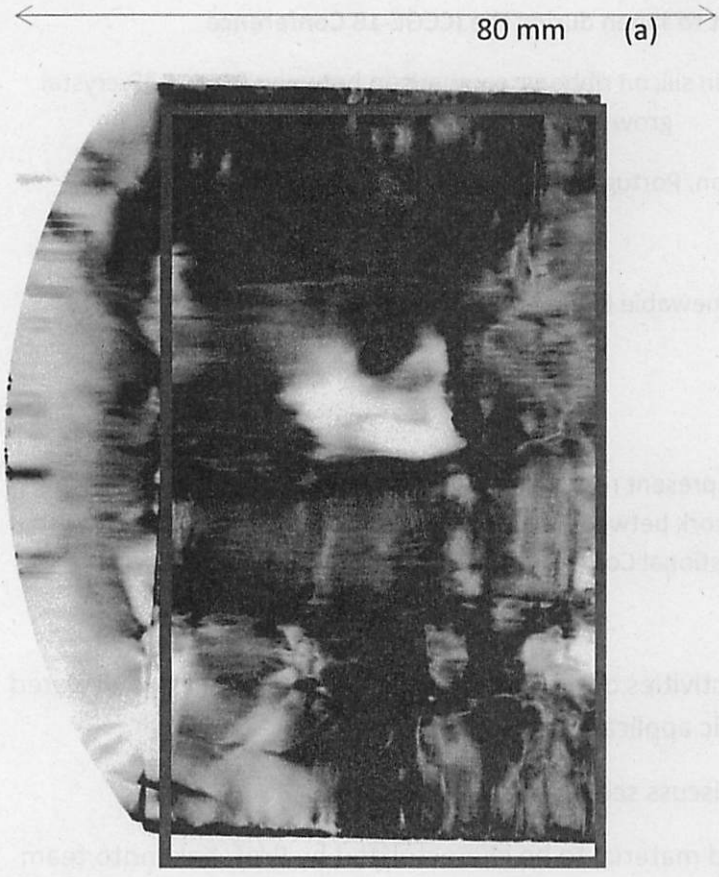

(b)

The figures are diffraction pattern from the sample of 2mm/min. We can identify the sample was curved in vertical direction from (a). There are many dislocations in the samples.

国際化推進共同研究概要

No.18

タ イ ト ル: Cold Crucible Czochralski (3CZ)

研究代表者: ZAIDAT, Kader

所内世話人: 柿本 浩一

実 施 期 間: 2016 年 8 月 5 日 ～8 月 13 日

研究概要: 2015 年はコールドクルーシブル法について、炭素や酸素のシリコンへの汚染について議論した。特に炭素と酸素の不純物レベルの定量的な議論をした。2016 年は、静磁場を用いることによりメルトの安定化に関する議論を行った。

Project: Cold Crucible Czochralski

Acronym: 3CZ

Scientific partners: SiMaP France/ RIAM Japan

1) Summary of the visit in 2015 at Kyushu University by Dr K. Zaidat

The goal of the visit was to present the scientific context (bibliography) at the Professor Kakimoto's group in order to discuss on the possibility to decrease the contamination (oxygen and carbon) during the Czochralski (Cz) process.

The visit was very fruitful for the two groups, in fact the Dr Zaidat has presented his idea on the possibility to use cold crucible in order to avoid oxygen during the Cz process. After some presentations on the different relative work on the topic it appears:

That the cold crucible will be a good compromise to avoid the contamination but the difficulty will be to adapt the thermal insulation around the ingot in order to avoid the thermal stress induced by the crucible.

The fluid flow induced inside a cold crucible will be the key parameter to achieve a large ingot with this technic.

According to the Professor Kakimoto, the dislocation density should be decrease (comparing the classical technic) only if the level of carbide and oxygen will be decrease at the same level of the Floating zone.

In conclusion, it was really a pleasure for the two groups to discuss on this critical point especially on the carbide and oxygen contamination. The two groups hope to continue to collaborate on this topic in the future.

2) Summary of the visit in 2016 at Nagoya during the International Conference of Crystal Growth and Epitaxy-2016

After a first visit in 2015 (see resume before), it was identified to find a solution on the control of the fluid flow inside a cold crucible. The two teams have discussed during the ICCGE conference organised by the Professor Kakimoto in order to propose a solution of this technical point.

The SIMAP team will try to add a static magnetic field in order to damped the liquid and decrease the velocity induced by the cold crucible. A first 2D model must be develop in order to understand the interaction between a static magnetic field and the electromagnetic field induced by the cold crucible.

国際化推進共同研究概要

No. 19

タイトル： Step dynamics on a vicinal surface with step-step attraction

研究代表者： TONCHEV Vesselin

(Institute of Physical Chemistry, Bulgarian Academy of Sciences, Bulgaria)

所内世話人： 寒川義裕

実施期間： 2016年8月1日～8月15日

薄膜結晶の開発を行うには成長表面における成長素過程、特にステップダイナミクスを理解することが重要である。本研究課題では、先ず、最近の研究成果をセミナー形式で発表し、議論を行った。セミナー発表の内容を次頁に記す。次に、共同研究者を含めて集中的な議論を行い、これまでに報告されているステップダイナミクスに関する研究論文を取り纏めた。得られた知見を「Mini-Review」として学術誌に公表した。公表した Mini-Review の概要は以下の通りである。

We review the studies on the scaling of the minimal step-step distance *l*min in the bunch with the bunch size N, *l*min $N^{-\gamma}$. We build our retrospective around the different values of the exponent γ obtained from models and experiments. It was mainly studied in the context of the electromigration driven instability on Si(111) vicinal surfaces. In this context, the full scaling relation is given in general form as *l*min ~ $(A/lcFN\,2)1/(n+1)$, where *A* is the magnitude of the step-step repulsions with range *n*, *F* is the electromigration force acting on the charged surface atoms and *l*c is a length-scale, characteristic for the regime of step bunching, diffusion-limited (DL) or attachment-detachment limited (KL).

Diffusion-limited vs. kinetics-limited regimes of step bunching

V. Tonchev
Institute of Physical Chemistry, Bulgarian Academy of Sciences, Sofia, Bulgaria

In this talk are presented numerical results from models of unstable vicinal crystal growth. In particular, they resolve the long-standing controversy between numerical results on the minimal step-step distance l_{min} in bunches and predictions of continuum theory - while the size-scaling exponent of l_{min} is found the same in diffusion-limited (DL) and kinetics-limited (KL) regime, and the time-scaling exponent of the bunch size N is predicted also to be the same (=1/2) in the relevant universality class, the scaling exponents of the bunch width W and l_{min} are predicted to distinguish in between. With extensive calculations on the model of Sato and Uwaha (SU) we solve the puzzle. Results from other models are discussed as well: vicinal Cellular Automata (vicCA), "sticky steps", etc. Especially, for the vicCA it is the time-scaling exponent of the macrostep size N_m that makes the difference.

In the prelude an account is given of the numerical results for the size-scaling of l_{min} in the two regimes for evaporation affected sublimation and the experimental evidence for DL regime. These are confronted with the predictions of the Pimpinelli et al. theory of universality classes in bunching and the correction of Krug et al. (KTSP) [1] to account for the differences in two regimes. Especially in the $\rho = -1$ universality class to which are expected to belong both vicinal evaporation and growth, only the time-scaling of W can distinguish between the two regimes. KTSP predict additionally that the time-scaling exponent of W in the KL regime is shifted with respect to the DL regime. Systematic numerical results for intermediate asymptotics from the SU-model [2] are obtained in the two regimes. These results show that the time-scaling exponents of W for the DL and for the KL are both shifted (differently) but the size-scaling exponent of l_{min} remains the same. Since SU model does not permit studying the infinite Ehrlich-Schwoebel barrier we study this using vicCA. In this model the time-scaling exponent of N is also invariant for DL and KL regimes (=1/3). Since there is no step-step repulsion incorporated in the model, besides bunching of mono-steps a macrostep formation is observed, thus l_{min}=0. The time-scaling exponent of N_m is 1/4 in the DL and 1/5 in the KL (see Fig. 1). We conclude with models of heteroepitaxial growth and a modification of the "sticky steps" model [3].

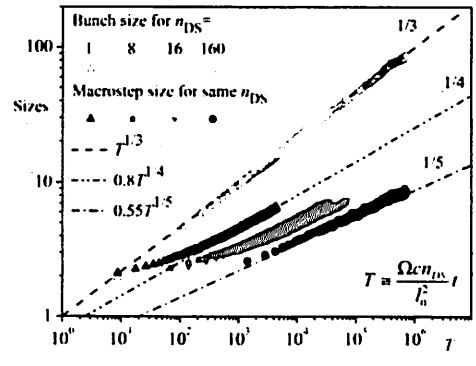

Fig. 1. Vicinal CA, time evolution of N and Nm varying number of diffusional steps per growth update, nDS = 1 (DL) to nDS = 160 (KL). Initial vicinal distance is l0 = 15, adatom concentration = 0.2.

References:

[1] Pimpinelli et al., Phys. Rev. Lett. **88**, 206103 (2002); Krug et al., Phys. Rev. B **71**, 206103 (2005).
[2] M. Sato and M. Uwaha, Surface science **493**, 494 (2001).
[3] N. Akutsu, Journal of Physics: Cond. Mat. **23**, 485004 (2011); N. Akutsu, AIP Advances, in print.

国際化推進共同研究概要

No.20

タ イ ト ル: Development and improvement multi-rotor wind turbine system

研究代表者: JAMIESON, PETER

所内世話人: 大屋 裕二

実 施 期 間: 2016 年 10 月 29 日 ～11 月 6 日

研究概要: 同一鉛直平面内に多数の風車をまとめて配置するマルチロータ風車が提唱されている. Jamieson らによるとマルチロータでは全体質量や発電コスト等を $1/\sqrt{n}$（nはマルチ個数）に抑えることが示されている. 我々は, このマルチロータ風車に当研究室で開発された高効率風車のつば付きディフューザ風車を採用したマルチレンズ風車（M-WLT）の開発に取り組んでいる. 本研究では並列配置のマルチレンズ風車の発電性能について報告し、最大で 14%程度のシステム出力増加を示したことを報告している。

Aerodynamics of Clustered, Diffuser Augmented Wind Turbines

Yuji Ohya[+1], Uli Goeltenbott[+2], Shigeo Yoshida[+1], and Peter Jamieson[+3]
[+1]Research Institute for Applied Mechanics, Kyushu University, Fukuoka, Japan
[+2]Dept.of Aeronautics and Astronautics, Graduate School of Engineering, Kyushu Univ., Fukuoka, Japan
[+3]University of Strathclyde, Glasgow, UK

Introduction

The wind turbine industry has seen innovations leading to growing size of turbines of currently over 140 meters in diameter. However, as pointed out by some recent studies, scaling of blades has its limitations and therefore advantages of multi-rotor system (MRS) concepts have been suggested by Jamison et al [Jamieson 2012]. We have been investigating the aerodynamics of brimmed diffuser wind turbines (called wind lens turbines) spaced closely together comprising a multi-rotor system. We spaced two or three of these turbines closely in an array perpendicular to the flow and measured each power output and drag. Several different wind lens configurations have been used, mainly varying the brim height and the diffuser shape.

Experimental Method and Results

Three wind-lens turbines in side-by-side arrangement

The 3-turbine configuration with WLTs in SBS arrangement shows a remarkable increase in average power output for practically all gap ratios s/D (gap ratio; s, gap; D, diffuser diameter) studied. The 3-WLT configuration can be seen in Figure 1 (left), while the results for the average power and drag coefficients of the 3-WLT configuration are shown on the right side in Figure 1. While the increase in power coefficient is notable for all gaps studied, the largest increase in ΔC_p, up to 14%, is achieved for the gap ratios at around s/D = 0.2 to 0.4. For the average drag coefficient, ΔC_d of the 3-WLT MRS shows increased values of up to 7% for gap ratios of s/D =0.2 to 0.4.

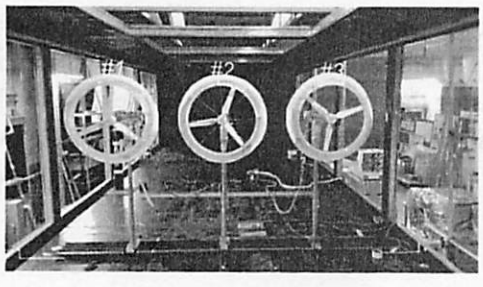

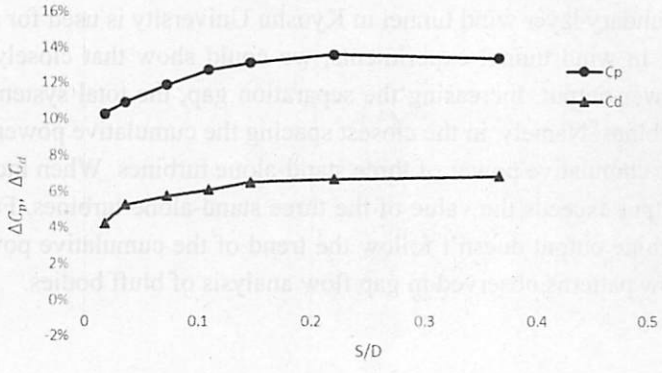

Figure 1: Experimental setup and variations in C_p and C_d for the configuration of three WLTs in SBS arrangement, compared to those for the stand-alone configuration.

The individual variations in C_{pi} and C_{di} for each WLT in the SBS arrangement are shown in Figure 2. The differences among the three WLT's power outputs and drags are clearly seen. Similar to the 2-WLT configuration, an increase in power coefficient in the 3-WLT configuration comes with an increase in drag coefficient. The average power coefficient increased up to 14% at s/D = 0.22. At the same gap, the average drag coefficient of the 3-WLT MRS increased by around 7% compared to the average of the single turbines in the stand-alone configuration. The increases in drag are much smaller than those in power output, showing half increase, as seen in Figures 1 and 2. The difference between ΔC_p and ΔC_d becomes larger compared to that for the 2-WLT configuration in SBS arrangement.

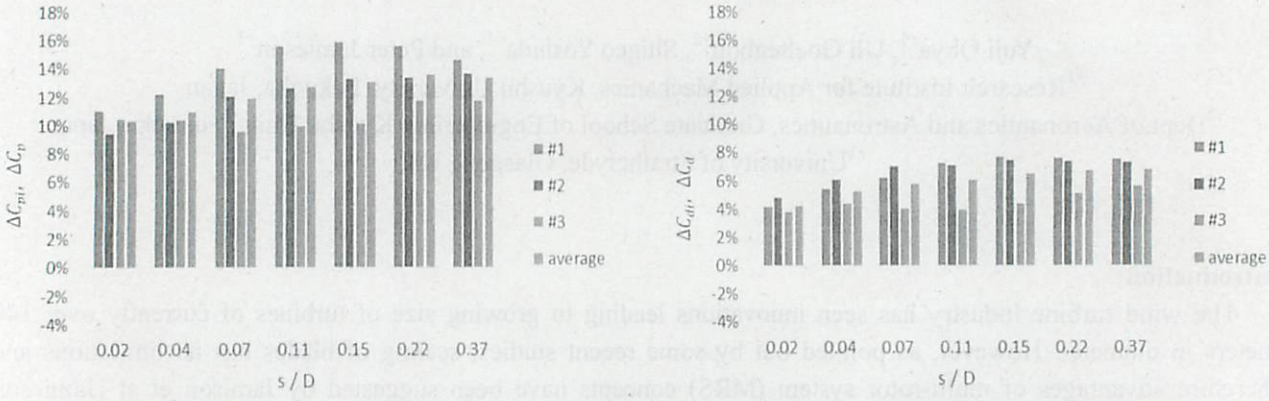

Figure 2: Individual variations in C_p and C_d for three WLTs in SBS arrangement, compared to those for the stand-alone configuration; left: C_p, right: C_d

Assuming that the difference in power coefficient of the three WLTs comes mainly from the biased gap flow, the flow pattern would show both gap flows to be biased to the left.

Conclusions

Multi-rotor systems (MRS) for wind turbine configurations have been studied for side-by-side (SBS) arrangements of conventional wind turbines and diffuser augmented wind turbines (DAWTs). First, the aerodynamics of two circular discs in SBS arrangement with close vicinity is investigated in order to better understand the aerodynamics of this configuration. Next, the power coefficient and the drag coefficient (thrust force) for two and three conventional turbines in SBS arrangements are investigated, followed by the same study for two and three brimmed-diffuser wind turbines (called Wind-Lens turbines, WLT) configurations. A large boundary layer wind tunnel in Kyushu University is used for all the experiments.

In wind tunnel experiments, we could show that closely spaced turbines have an influence on each other's power output. Increasing the separation gap, the total system power output exceeded the sum of the stand-alone turbines. Namely, in the closest spacing the cumulative power of all three turbines is almost the same, compared to the cumulative power of three stand-alone turbines. When increasing the gap between the turbines, the total power output exceeds the value of the three stand-alone turbines. Further it was observed that the individual power of a turbine output doesn't follow the trend of the cumulative power output. These phenomena can be explained with flow patterns observed in gap flow analysis of bluff bodies.

Acknowledgement

This work was supported in part by the Collaborative Research Program of Research Institute for Applied Mechanics, Kyushu University.

日本語概要

同一鉛直平面内に多数の風車をまとめて配置するマルチロータ風車が提唱されている．Jamieson らによるとマルチロータでは全体質量や発電コスト等を $1/\sqrt{n}$（n はマルチ個数）に抑えることが示されている．我々は，このマルチロータ風車に当研究室で開発された高効率風車のつば付きディフューザ風車を採用したマルチレンズ風車（M-WLT）の開発に取り組んでいる．本研究では並列配置のマルチレンズ風車の発電性能について報告し、最大で 14%程度のシステム出力増加を示したことを報告している。

Published papers list

[1] "Power augmentation of shrouded wind turbines in a multi-rotor system"
Proceedings of 2nd International Conference On Next Generation Wind Energy (2nd ICNGWE), Lund, Sweden, August 24-26, 2016. Yuji Ohya, Junpei Miyazaki, Uli Göltenbott, Takashi Karasudani, Shigeo Yoshida

[2] "Coherence Effects on the Power and Tower Loads of a 7 x 2 MW Multi-Rotor Wind Turbine"
Energies 9(9):742, 2016. doi:10.3390/en9090742, Shigeo Yoshida, Uli Goltenbott, Yuji Ohya, Peter Jamieson

[3] "Flow interaction of diffuser augmented wind turbines" Proceedings of Making Torque from Wind 2016, Munich, Journal of Physics: Conference Series 753 (2016) 022038, Uli Goeltenbott, Yuji Ohya, Shigeo Yoshida, Peter Jamieson

[4] "Arrangements of three diffuser augmented wind turbines in a multi-rotor system", Proceedings of the World Wind Energy Conference 2016, Tokyo, Uli Goeltenbott, Yuji Ohya, Shigeo Yoshida, Peter Jamieson

[5] "Multi Rotor-System using Diffuser Augmented Wind Turbines for Power Increase"
Proceedings of the World Wind Energy Conference 2016, Tokyo. Akio Munakata, Jumpei Miyazaki, Uli Goeltenbott, Yuji Ohya, Takanori Uchida

[6] "Power augmentation of shrouded wind turbines in a multi-rotor system" American Society of Mechanical Engineering, Journal of Energy Resources and Technology, vol.139, 051202-1 2017. Yuji Ohya, Junpei Miyazaki, Uli Göltenbott, Koichi Watanabe.

[7] "Aerodynamic interaction of diffuser augmented wind turbines in multi-rotor systems"
Journal of Renewable Energy 2017 (in print), Uli Goeltenbott, Yuji Ohya, Shigeo Yoshida, Peter Jamieson